AGU PUBLICATIONS

Geophysical Research Letters

RESEARCH LETTER
10.1002/2016GL071134

Key Points:
- We investigate subpolar decadal temperature variability associated with the North Atlantic Current
- This variability covaries with Atlantic and Pacific Ocean decadal climate modes
- Atlantic climate variability leads/amplifies that of the Pacific and its associated teleconnections

Supporting Information:
- Supporting Information S1
- Data Set S1

Correspondence to:
L. Chafik,
leon.chafik@uib.no

Citation:
Chafik, L., S.Hakkinen, M. H. England, J. A. Carton, S. Nigam, A. Ruiz-Barradas, A.Hannachi, and L. Miller (2016), Global linkages originating from decadal oceanic variability in the subpolar North Atlantic, *Geophys. Res. Lett.*, *43*, 10,909–10,919, doi:10.1002/2016GL071134.

Received 30 JUN 2016
Accepted 3 OCT 2016
Accepted article online 5 OCT 2016
Published online 21 OCT 2016

Global linkages originating from decadal oceanic variability in the subpolar North Atlantic

L. Chafik[1,2], S. Häkkinen[3], M. H. England[4], J. A. Carton[5], S. Nigam[5], A. Ruiz-Barradas[5], A. Hannachi[6], and L. Miller[1]

[1]NOAA/NESDIS Center for Satellite Application and Research, College Park, Maryland, USA, [2]Cooperative Institute for Climate and Satellites, University of Maryland, College Park, Maryland, USA, [3]NASA Goddard Space Flight Center, Greenbelt, Maryland, USA, [4]Australian Research Council Centre of Excellence for Climate System Science and Climate Change Research Centre, University of New South Wales, Sydney, New South Wales, Australia, [5]Department of Atmospheric and Oceanic Science, University of Maryland, College Park, Maryland, USA, [6]Department of Meteorology, Stockholm University, Stockholm, Sweden

Abstract The anomalous decadal warming of the subpolar North Atlantic Ocean (SPNA), and the northward spreading of this warm water, has been linked to rapid Arctic sea ice loss and more frequent cold European winters. Recently, variations in this heat transport have also been reported to covary with global warming slowdown/acceleration periods via a Pacific climate response. We here examine the role of SPNA temperature variability in this Atlantic-Pacific climate connectivity. We find that the evolution of ocean heat content anomalies from the subtropics to the subpolar region, likely due to ocean circulation changes, coincides with a basin-wide Atlantic warming/cooling. This induces an Atlantic-Pacific sea surface temperature seesaw, which in turn, strengthens/weakens the Walker circulation and amplifies the Pacific decadal variability that triggers pronounced global-scale atmospheric circulation anomalies. We conclude that the decadal oceanic variability in the SPNA is an essential component of the tropical interactions between the Atlantic and Pacific Oceans.

1. Introduction

The multidecadal variability of the North Atlantic Ocean has a strong signal in the sea surface temperature with many global climate linkages [*Enfield et al.*, 2001; *Knight et al.*, 2006]. An even stronger multidecadal signal can be found in the subpolar temperatures and salinities, where the Atlantic Water inflow variations constitute an essential part in the variability [*Hátún et al.*, 2005; *Häkkinen et al.*, 2011a; *Reverdin*, 2010]. The atmospheric forcing in the subpolar North Atlantic Ocean is dominated by the variability of the North Atlantic Oscillation (NAO), i.e., the leading mode of atmospheric variability in the North Atlantic sector, which modulates the atmosphere-ocean momentum and heat exchanges on a range of temporal scales. The subpolar ocean variability thus appears to be tightly connected to atmospheric forcing and associated basin-scale circulation changes, which together force the subpolar ocean properties toward extremes [*Lozier et al.*, 2008, 2010], either to warm-saline or cold-fresh conditions on multidecadal scales. These regime changes have recently been argued to be important for global mean surface temperature warming acceleration and hiatus [*Chen and Tung*, 2014; *Drijfhout et al.*, 2014] (Figure S1 in the supporting information).

The temporary decadal-long global warming slowdown just after the turn of the century has received much attention from the climate community [*Meehl et al.*, 2011; *Trenberth and Fasullo*, 2013; *Kosaka and Xie*, 2013; *Watanabe et al.*, 2014; *Trenberth et al.*, 2014; *England et al.*, 2014; *McGregor et al.*, 2014; *Song et al.*, 2014; *Maher et al.*, 2014; *Steinman et al.*, 2015; *Fyfe et al.*, 2016]. Natural internal variability can temporarily influence and cause a "pause" in an otherwise upward global mean air temperature trend [*Held*, 2013; *Trenberth*, 2015]. Numerous reasons, mainly centered around the low-frequency Pacific climate variability, have been offered [*Kosaka and Xie*, 2013; *Watanabe et al.*, 2014; *Trenberth et al.*, 2014; *England et al.*, 2014; *McGregor et al.*, 2014; *Maher et al.*, 2014]. Other studies [*Katsman and van Oldenborgh*, 2011; *Balmaseda et al.*, 2013; *Chen and Tung*, 2014; *Drijfhout et al.*, 2014] have also suggested the redistribution of heat across multiple basins and into the depths of the oceans as alternate explanations for the missing heat offsetting the global warming acceleration.

A growing number of studies have highlighted the importance of the tropical Atlantic warming trend since the mid-1990s in generating the pronounced eastern Pacific cooling and negative Interdecadal Pacific Oscillation trend that dominated for more than a decade since around 2001 [*Kucharski et al.*, 2011; *Chikamoto et al.*, 2012; *McGregor et al.*, 2014; *Kucharski et al.*, 2015; *Li et al.*, 2015]. *Chikamoto et al.* [2012], for example, pointed out that the stepwise climate shifts in the Pacific are a lagged response to the basin-scale warming/cooling of the North Atlantic. A warming of the Atlantic Ocean induces a basin-scale sea surface temperature seesaw with the Pacific [*Wang*, 2006], which in turn reorganizes the position of the Walker circulation, strengthens the easterly trade winds [*Lindzen and Nigam*, 1987; *England et al.*, 2014], and influences the Pacific decadal variability, as suggested recently by *McGregor et al.* [2014]. The latter study further finds that East Pacific cooling can induce a tropical warming response in the Atlantic, suggesting two-way interbasin coupling. The Atlantic and Pacific are thus linked through this large-scale transbasin variability that may, initially, be induced by North Atlantic Ocean dynamics via a slowdown, or spin-up, of the Atlantic meridional circulation and the associated northward heat transport [*Timmermann et al.*, 2007; *McCarthy et al.*, 2015; *Robson et al.*, 2016; *Zhang et al.*, 2016].

We focus the present study on understanding the role of the subpolar North Atlantic Ocean (SPNA) in driving this Atlantic-Pacific interconnection. Our approach is to identify the potential source leading to a regime shift of Atlantic Water subsurface temperatures in the SPNA. These shifts are found to be associated with a decadal-scale progression of heat anomalies from the Gulf Stream region and revealed to coincide with sea surface temperatures extending to cover most of the subpolar and tropical North Atlantic. As a result of this basin-wide climate change, a large-scale Atlantic-Pacific surface temperature gradient, which correlates well with the strength of the Walker circulation, is generated and the Pacific decadal variability is amplified. These results are discussed in detail below and derived from several observational data sets as described in the next section.

2. Data and Methods

To better understand the low-frequency temperature variability in the SPNA, we construct a subsurface temperature index in the SPNA that is colocated with the core of the North Atlantic Current (see Figure 1). To do this, we first construct a temperature cross section centered along 59.5°N by averaging associated grid points latitudinally between 58°N and 61°N. These are averaged along a line parallel to the Reykjanes Ridge and not in the north-south direction [*Chafik et al.*, 2014]. Second, we omit the upper 300 m, partly due to the large month-to-month variability, to ensure that the temperature variability captured is associated with that of the North Atlantic Current. Third, at every time step, we area average temperature corresponding to salinity larger than the 35.1 climatological isohaline. The resulting index, termed Atlantic Water Temperature (AWT), is thus a volumetrically averaged subsurface temperature of Atlantic Water along the pathway of the North Atlantic Current in the SPNA.

The temperature data are based on the monthly mean objectively analyzed hydrographic data from the UK Met Office, EN4 [*Good et al.*, 2013]. This data set is also used to calculate ocean heat content (OHC) in the upper 657 m of the water column:

$$\mathrm{OHC} = \rho_0 c_p \int_5^{657} T(z)\mathrm{d}z, \tag{1}$$

where ρ_0 and c_p are the seawater density and specific heat capacity, respectively. In situ observations were rather sparse before the 1950s and mostly relax to climatology. We therefore rely on the period between 1950 and 2012 for our analyses. Complementary to OHC, we also use sea surface temperatures (SSTs) from the ERSSTv4 data set [*Huang et al.*, 2016]. Geopotential height and tropical Pacific winds are based on the twentieth century National Centers for Environmental Prediction/National Center for Atmospheric Research reanalysis [*Compo et al.*, 2011]. OHC, SSTs, geopotential heights, and winds have been deseasoned and linearly detrended before the analyses. We also use several climate indices publicly available on the NOAA website. These are based on similar data sets as all other variables. The indices are the NAO, Atlantic Multidecadal Oscillation (AMO), and Pacific Decadal Oscillation (PDO). All variables and indices have been smoothed using a 25 month running mean prior to the analyses, unless otherwise stated. Given this low-pass filtering, the significance of the Atlantic-Pacific lag-lead SST correlations is assessed using 5000 Monte Carlo simulations

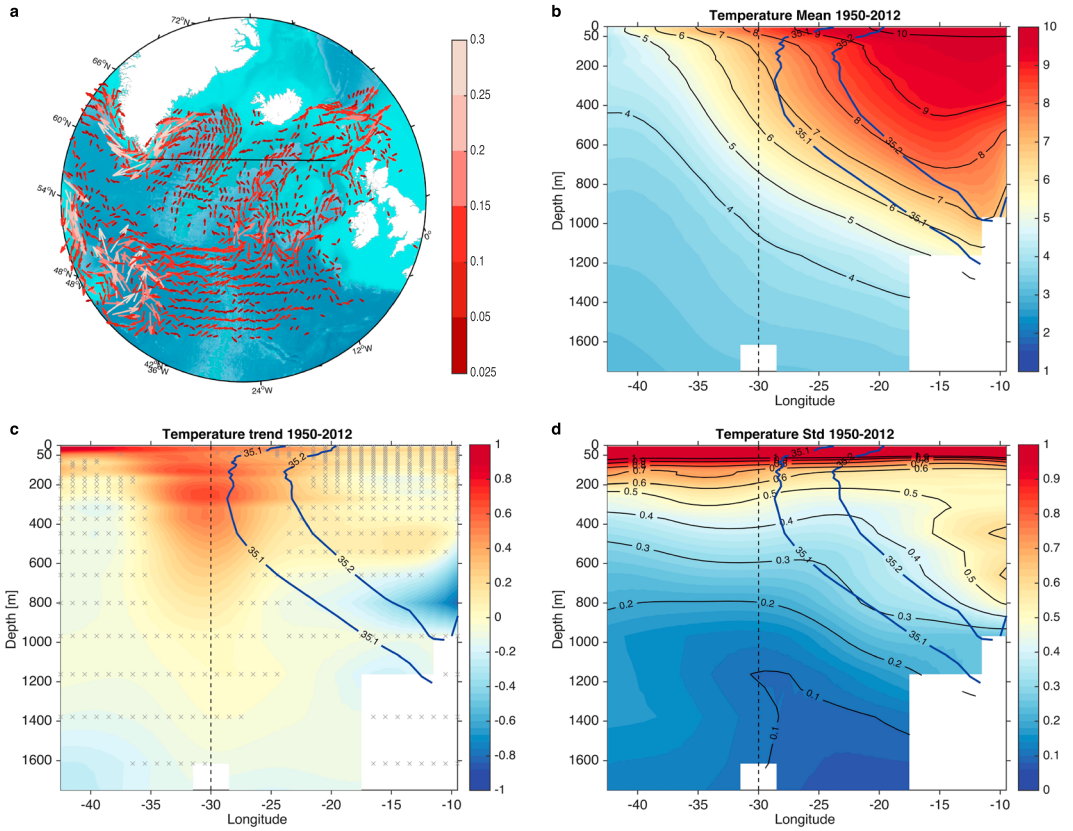

Figure 1. Temperature climatology, trend, and variability in the SPNA between Scotland and Greenland. (a) Time-mean surface currents (m s^{-1}) derived from altimetry. The 1950–2012 (b) climatology, (c) trend, and (d) standard deviation of potential temperature (°C) from EN4 in depth-longitude coordinates. The 35.1 and 35.2 climatological isohalines are indicated by the blue contours. The cross section used to construct Figures 1c and 1d is shown in black in Figure 1a and is a result of averaging over latitude bands between 59 and 61°N. The latitudinal averaging of the potential temperature is performed along a slope parallel to that of the Reykjanes Ridge following the orientation of the currents. The dashed line at 30°W represents the Reykjanes Ridge. The gray stipplings in Figure 1c denote nonsignificant grid points at the 99% confidence level based on the modified Mann-Kendall test [*Hamed and Rao*, 1998].

[*Ebisuzaki*, 1997] at the 99% confidence level. The random-phase method in the Monte Carlo significance test resamples the data in the frequency domain, which preserves its autocorrelation and power spectrum, but generally is as robust as a two-sided *t*-test [*Von Storch and Zwiers*, 2001].

3. Results

3.1. Climatology and Long-Term Changes Across the SPNA

The time-mean surface currents from satellite altimetry (Figure 1a) reveal the flow toward the Nordic Seas and the Labrador Sea, respectively, following the upper limb of the Atlantic meridional overturning circulation [*Chafik et al.*, 2015; *Buckley and Marshall*, 2016]. In the upper 400 m, equal amounts of water (~ 8×10^6 m^3 $s^{-}1$) are transported by these branches [*Chafik et al.*, 2014], which are effectively separated and topographically organized by the Reykjanes Ridge at 30°W. East of this ridge, the isotherms reach deeper due to the presence of warm Atlantic Water associated with the North Atlantic Current as indicated by the gradual shoaling and cooling toward the west (Figure 1b). The Mann-Kendall test [*Hamed and Rao*, 1998] indicates a significant upward temperature trend in the SPNA (Figure 1c). The strong warming of the subpolar region is likely associated with the weakening of the gyre circulation [*Häkkinen and Rhines*, 2004; *Lohmann et al.*, 2009; *Häkkinen et al.*, 2013] but may also be partly anthropogenically forced [*Stocker et al.*, 2013]. The standard deviation of the monthly data shows that the largest temperature variability between Scotland and Greenland during the past 63 years is found near the surface and also subsurface in the Iceland Basin (Figure 1d), which is consistent with the path of the North Atlantic Current.

3.2. North Atlantic Decadal Climate Shifts

The subsurface temperature index corresponding to Atlantic Water in the SPNA captures the largest variability associated with the core of the North Atlantic Current (Figure 1). It exhibits pronounced decadal climatic shifts (Figure 2a) associated with warm and cold periods lasting for about 17 years as confirmed by its power spectrum (Figure 2b) and projects onto an ocean heat content dipole pattern between the subpolar gyre and the Gulf Stream region (Figure 2c). This pattern is remarkably similar to that based on subsurface temperatures reported to be induced by the meridional overturning circulation [*Zhang*, 2008]. In the SPNA, the warm/cold period thus corresponds to a weaker/stronger than average subpolar gyre and higher/lower heat content [cf. *Häkkinen et al.*, 2013, Figure 5]. In the Gulf Stream region, however, the cold and warm anomalies have been associated with southward and northward shifts of the Gulf Stream position induced by variations in the meridional overturning circulation [*Joyce and Zhang*, 2010], leakage of slope waters [*Rossby and Benway*, 2000], and temporal variability of the NAO [*Frankignoul et al.*, 2001]. The preceding studies elucidate changes in the Gulf Stream controlled by both atmospheric forcing, mainly associated with the NAO, and changes in the meridional overturning circulation in a region where the circulation of the subpolar and subtropical gyres interacts. The impact from these two sources of variability is difficult to separate as they might be induced by the same climatic forcing.

Based on the progression of ocean heat content in the top 700 m (Figure 3), we shed some light on how the warm-to-cold (Figures 3a–3c) and cold-to-warm (Figures 3d–3f) AWT phase transitions may occur. Propagating anomalies from the subtropics, with an amplification in the SPNA gyre, are observed. It is noteworthy that during a cold-to-warm (warm-to-cold) regime transition, a cold (warm) anomaly from the subpolar gyre moves southward along the western boundary, while concurrently, a warm (cold) anomaly from the Gulf Stream region advects along the mean path of the North Atlantic Current toward the eastern SPNA and subsequently around the subpolar gyre following the mean circulation. Figure S4 further suggests that this ocean heat content dipole is strengthened, outside these transition periods, under persistent NAO forcing.

Using an ensemble of initialized decadal prediction experiments, *Yeager et al.* [2012] pointed out that SPNA temperature regime shifts can be tied to the low-frequency advection of heat anomalies associated with the meridional overturning circulation and NAO-related buoyancy forcing [*Robson et al.*, 2012, 2016]. Recently, *McCarthy et al.* [2015] reported that the decadal evolution of North Atlantic heat content is affected by changes in the ocean circulation [e.g., *Grist et al.*, 2010], which responds to the NAO, through excursions in the subtropical-subpolar gyre boundary and anomalous circulation in the intergyre-gyre region [*Marshall et al.*, 2001; *Eden and Willebrand*, 2001; *Herbaut and Houssais*, 2009]. Through a similar mechanism, *Wouters et al.* [2012] found that temperature anomalies from the subtropics to the subpolar region, similar to that in Figure 3, are advected cyclonically toward the Labrador Sea where they influence the deep water formation and hence the overturning circulation. The advection of Gulf Stream waters into the subpolar gyre via the eastern boundary has also been proposed to be induced by changes in the strength and horizontal shape of the subpolar and subtropical gyres due to low-frequency variations in the wind-stress curl [*Häkkinen and Rhines*, 2009; *Häkkinen et al.*, 2011a] (Figure S4). It is thus expected that these decadal heat anomalies flowing into the SPNA are associated with spin-up or slowdown of the overturning and/or the wind-driven gyre circulation, and they coincide with changing phase of the AMO/AWT.

3.3. AWT Synchronizes Atlantic and Pacific Climate Variability

To demonstrate large-scale features and to better understand the global linkages associated with AWT, composite analyses using anomalies of SSTs and nonzonal geopotential heights at 200 hPa are constructed (Figure 4) (Figures S5 and S6). The latter is informative in terms of highlighting tropical-extratropical linkages associated with the flux of atmospheric Rossby waves connecting the Pacific to the Atlantic [*Ding et al.*, 2014]. The SST patterns (Figure 4a), both in the North Atlantic and Pacific, reflect horseshoe characteristics, which generally mirror the leading modes of SST variability in the North Atlantic and Pacific widely known as the AMO [*Enfield et al.*, 2001] and PDO [*Mantua*, 1997], respectively. In the SPNA, SST anomalies show a basin-wide warming/cooling associated with anomalous positive/negative phases of AWT (Figure S7). These anomalies tend, particularly in the western subpolar gyre, to be strongly enhanced by air-sea fluxes under specific atmospheric regimes [see, e.g., *Barrier et al.*, 2015; *Häkkinen et al.*, 2011b].

From a global perspective, AWT is seen to be associated with a teleconnection pattern originating from the tropical Pacific (Figure 4b), which expresses itself well in the upper troposphere at 200 hPa (anomalies at this

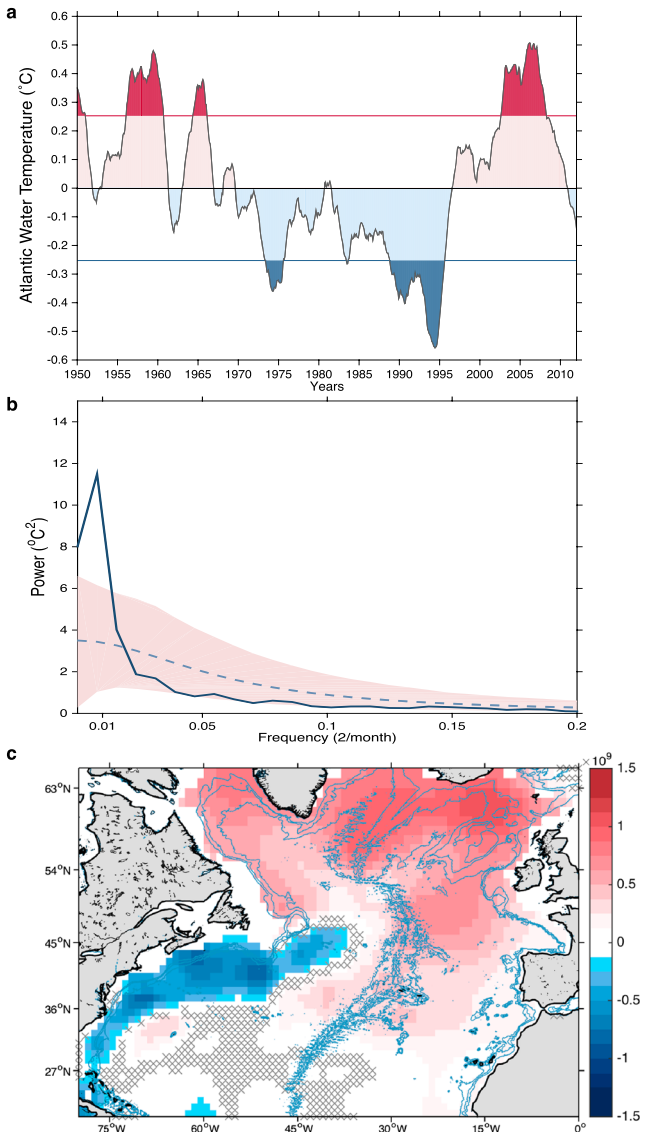

Figure 2. Characteristics of AWT variability. (a) AWT index (°C) during the 1950–2012 period (shading). The raw AWT (Figure S2) has been deseasoned, detrended, and smoothed with a 25 month running mean. Dark blue and red indicate anomalous periods (larger and smaller than 1 standard deviation) of AWT. (b) Power spectrum of the raw AWT using the Welch estimation method (solid line). The dashed line shows the power spectrum of the first-order autoregressive model, AR(1), having the same lag-1 autocorrelation as the AWT time series. The shading represents the 99% confidence limits obtained by generating 1000 random AR(1) models of the AWT series. Note the significant power in the low-frequency band of the spectrum with decadal and longer time scales. There is a particular peak at 17 year period. (c) Regression of ocean heat content anomalies (J m^{-2}) onto AWT, where a dipole between the Gulf Stream and subpolar gyre is highlighted. Gray crosses indicate the nonsignificant regions below the 99% confidence level assessed using a two-sided *t*-test.

level represent the thickness of the troposphere, and hence, colder/warmer than average SST anomalies in the tropical Pacific are characterized by anomalously lower/higher pressure throughout the tropics and troposphere depth) in the form of a quasi-stationary Rossby wave pattern bridging the tropical Pacific and the Atlantic through the sub-Arctic. The tropical Pacific forces and sets up a coherent wave train structure (it is noteworthy that the first negative geopotential height anomaly center is typically located off the equator at subtropical latitudes away from the thermal source [*Horel and Wallace*, 1981; *Trenberth et al.*, 1998]) leading, in part, to an eastward shift and a deepening of the Aleutian Low as well as an intensified high-pressure ridge in the North Atlantic reminiscent of a negative NAO-like mode. For example, *Ding et al.* [2014] linked the

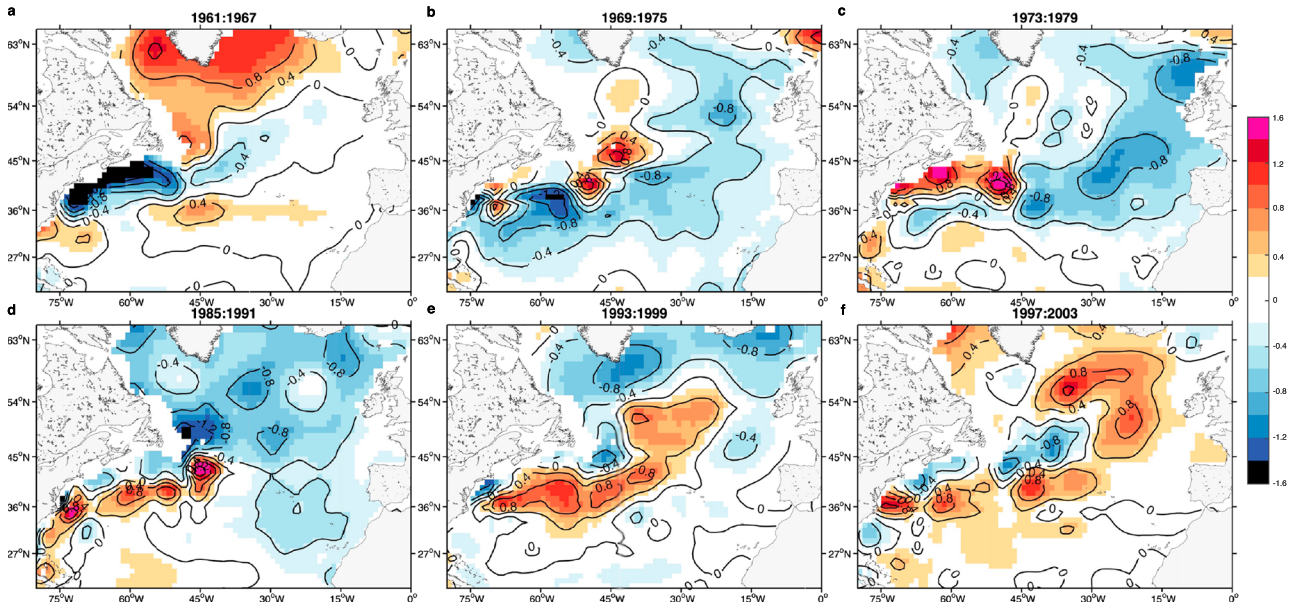

Figure 3. Spatial progression of ocean heat content anomalies (J $m^{-2} \times 10^9$) associated with the temperature transitions reflected in AWT. The 7 year time windows for the warm-to-cold transition are averaged for (a) 1961–1967, (b) 1969–1975, and (c) 1973–1979 periods. For the cold-to-warm transition the averaging is done for the periods (d) 1985–1991, (e) 1993–1999, and (f) 1997–2003 (see the entire 1949–2013 evolution in Figure S3). Figures 3a and 3d show averaging during a strictly warm/cold phase, while Figures 3b and 3e represent an intermediate phase before the transition to a strictly cold/warm state as shown in Figures 3c and 3f. These time windows have been chosen in a symmetric fashion (see Figure 2a) to visualize the transition from warm-to-cold and cold-to-warm periods. We, therefore, had to overlap the intermediate period in Figures 3c and 3d.

pronounced surface warming in northeastern Canada and Greenland to the negative NAO trend, which was found to be a response to the above mentioned anomalous Rossby wave train activity originating in the tropical Pacific. Moreover, *Trenberth et al.* [2014] pointed out that most atmospheric anomalies during the recent hiatus are of tropical Pacific origin and resemble the PDO.

3.4. Is the Atlantic Leading the Pacific?

We observe that an SST signal first originates within the Gulf Stream region outside Cape Hatteras almost a decade (maximum correlation at ~4–6 years) before it reaches the SPNA (Figure 5a). The propagation pattern is compatible with that of ocean heat content (Figure S3). Note, however, that the signal also shows a propagation toward the tropical Atlantic. This is consistent with a horseshoe pattern where the temperature signal communicates with both the SPNA and the subtropics following the subpolar and subtropical gyres, respectively, an impression reinforced by regressing SSTs onto the AWT at different lags (Figures S8 and S9). A discussion on similarities and differences between AWT and AMO is offered in the supporting information.

The atmospheric variability in the North Atlantic is notably leading the AWT (Figure 5b). This is manifested in the upper troposphere by a tripole pattern which resembles that induced by the NAO (Figure 5b). Whether this is a lagged response to the basin-wide spread of SST anomalies originally initiated in the subtropics along the Gulf Stream path is beyond the scope of the present study. Several studies have, however, pointed out that AMO-like SST anomalies are able to modify the strength of the large-scale atmospheric circulation through shifts in the position of the baroclinic zone [*Czaja and Frankignoul*, 1999, 2002; *Gastineau and Frankignoul*, 2012; *Peings and Magnusdottir*, 2014; *Gastineau and Frankignoul*, 2015].

In the Pacific, however, oceanic and atmospheric variability are evidently lagging changes in the Atlantic (Figure 5b). Subtropical Pacific SSTs lag AWT with a maximum correlation of 1–3 years (Figure 5b), and the associated atmospheric thickness (850–200 hPa) shows a dipole pattern between the subtropics and extratropics (as a response to the large-scale SST pattern or PDO) extending from the Pacific into the Atlantic, thereby completing a full interbasin Rossby wave train picture (Figure 5d). In the tropics and subtropics, an interbasin dipole pattern in the pressure field between the Atlantic and Pacific [see, e.g., *McGregor et al.*, 2014;

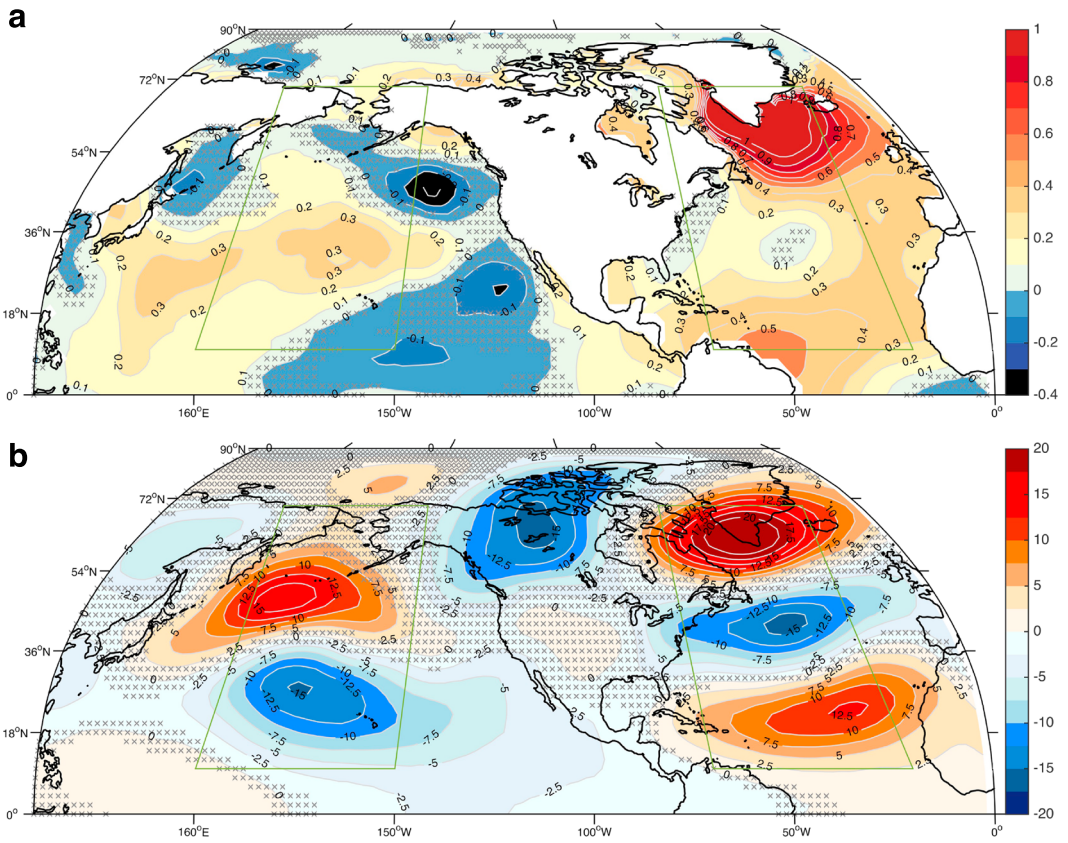

Figure 4. AWT variability and its global linkages. AWT-based composite analysis of (a) SST anomalies (°C), and (b) nonzonal 200 hPa geopotential height anomalies (gpm). The composite is based on the difference between events larger and less than 1 standard deviation for the anomalously warm and cold AWT periods (dark red/blue in Figure 2a), respectively. Nino3.4 has been removed prior to the analysis. Gray crosses indicate the nonsignificant regions below the 99% confidence level assessed using a two-sided *t* test.

Chikamoto et al., 2015] is observed and persists there for an extended number of years. Our results thus suggest that the Atlantic amplifies the negative and positive anomalies of the internally generated variability of the PDO [see, e.g., *Chikamoto et al.*, 2012].

In conclusion, we show evidence that SPNA and tropical Atlantic SST anomalies are consistent with an advective origin due to changes in the ocean circulation [*Zhang et al.*, 2016; *Drews and Greatbatch*, 2016]. However, the Pacific decadal variability is not amplified until temperature anomalies have connected with the tropical Atlantic and the basin-scale pattern linked to AWT is fully developed. This results in an interbasin gradient or seesaw between the Atlantic and Pacific and a shift in the Walker circulation (Figure 5e). This transbasin variability (Atlantic warming/cooling-Pacific cooling/warming) has been recently suggested to have amplified the recent Pacific cooling and hence a slowdown in global mean surface air temperature [*McGregor et al.*, 2014].

To further understand the physical link between the Atlantic and Pacific, we construct an interbasin SST gradient or transbasin variability following *McGregor et al.* [2014]. This index does not only combine information on how the basin-average Atlantic and Pacific SSTs vary but also mirrors the strength of the trade winds and hence shifts of the Walker circulation (Figure S10). We note that the negative and positive phases of this index covary with the cold and warm periods of AWT with a significant lag of 21 months. The warming (cooling) of the North Atlantic Basin reflected by positive AWT phase leads to a positive (negative) SST transbasin variability, i.e., difference between the Atlantic and Pacific. As a result, sinking/rising motion and upper level convergence/divergence occurs in the central Pacific/Atlantic and easterly winds are strengthened in the central western Pacific region, which amplifies the cooling in the tropical Pacific [*England et al.*, 2014; *McGregor et al.*, 2014; *Kucharski et al.*, 2015; *Li et al.*, 2015], and vice versa. Thus, Atlantic climate variability plays an important role for the position of the Walker circulation and contributes to the generation of Pacific decadal variability.

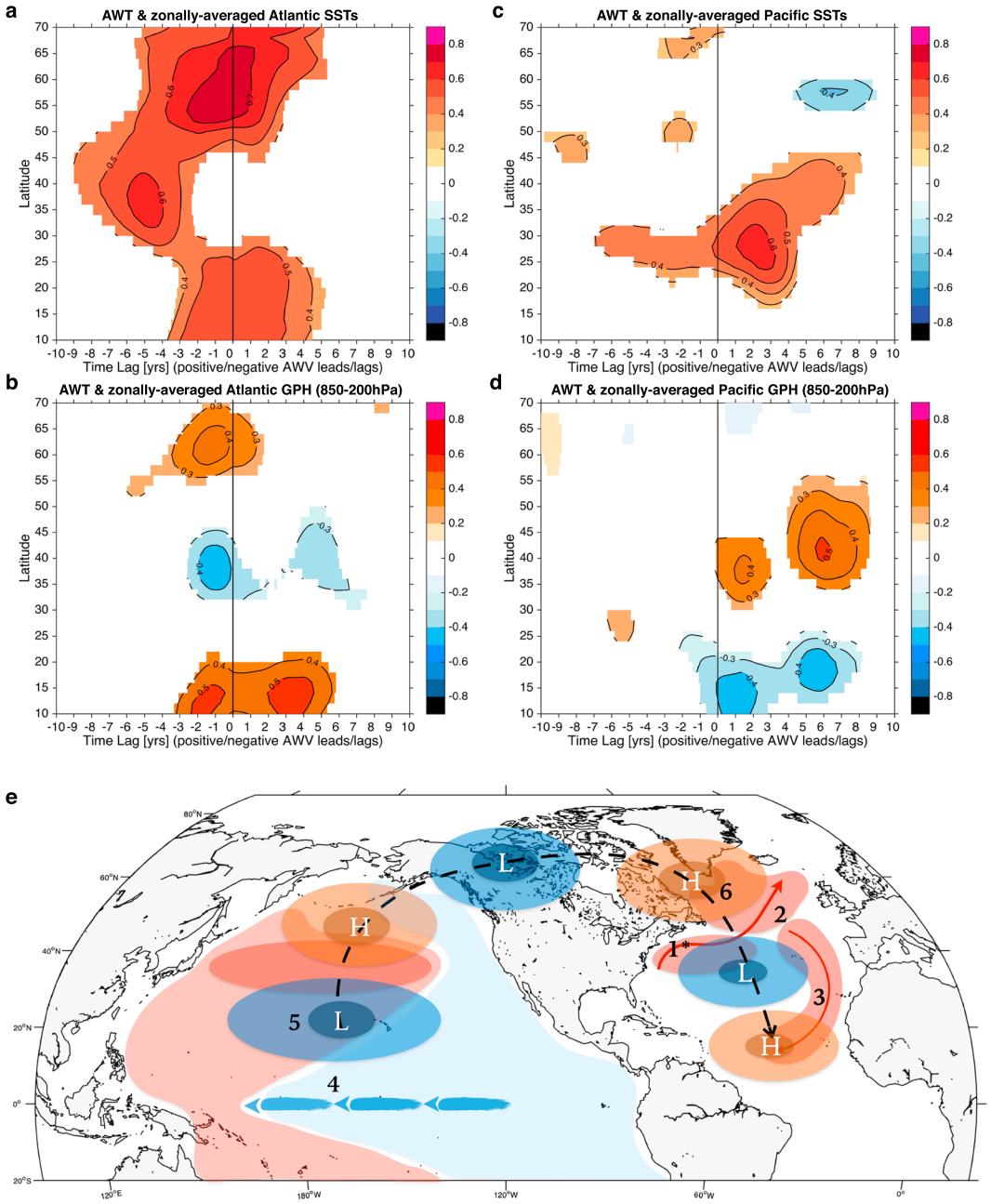

Figure 5. AWT and Atlantic-Pacific connectivity. Lag-lead correlation in years based on AWT and zonally averaged (a) Atlantic SST, (b) Pacific SST, (c) Atlantic, and (d) Pacific geopotential height (GPH) averaged between 850 and 200 hPa. The zonal averaging is performed within the green boxes (cf. Figure 4). The shaded regions (Figures 5a–5d) are statistically significant at the 99% confidence level based on the random-phase test using 5000 Monte Carlo simulations. Nino3.4 has been removed prior to the analysis. (e) Schematics of the global linkages for a typical warm phase, where (1) the Gulf Stream region appears to be the main source of the warm anomaly, which (2) progresses toward the SPNA and also (3) reaches the tropical Atlantic (Figures S8 and S9). (4) This creates a large-scale SST gradient between the Atlantic and Pacific that modifies the Walker circulation and strengthens the trade winds. (5) The negative PDO phase is hence amplified, which excites a flux of Rossby waves into the Atlantic. (6) This organization reinforces the high-pressure anomaly over the subpolar gyre region.

4. Summary and Conclusions

The purpose of this study has been to gain a better understanding of the interbasin linkages between the Atlantic and Pacific in relation to the decadal variability that characterizes AWT in the SPNA (Figure 2). This is found to be associated with a decadal-scale progression of heat content anomalies from the subtropics into the subpolar gyre and coincide with basin-wide, AMO-like, climatic changes. Ocean circulation is evidently playing a role in inducing the observed North Atlantic changes [*Zhang et al.*, 2016; *Drews and Greatbatch*, 2016]. The strength of the meridional overturning [*Robson et al.*, 2016] and wind-driven circulation [*Häkkinen et al.*, 2011a; *McCarthy et al.*, 2015] are expected to dominate the evolution of ocean heat content anomalies; however, their relative roles are not yet fully understood.

Here we have shown that AWT in the SPNA synchronizes with the dominant modes of climate variability in the Atlantic and Pacific and appears to contribute to the low-frequency Pacific decadal variability with a maximum lag of ~2–3 years (Figure S7). While our analyses were based entirely on observations, and are restricted to a limited period of reliable observations, evidence can also be found in forced atmosphere and coupled climate model experiments, wherein imposed SST anomalies are applied. For example, *Chikamoto et al.* [2012] found that Pacific stepwise climate shifts are found to lag changes in Atlantic SSTs by around 2 years. It is, however, important to recognize that this interbasin connection occurs via the tropics after extratropical SSTs have communicated with the tropical Atlantic [*Guan and Nigam*, 2009; *Ruiz-Barradas et al.*, 2013]. This, in turn, induces the Atlantic-Pacific SST gradient necessary to modify to the Walker circulation and can translate into a multiyear persistence predictive skill [*McGregor et al.*, 2014; *Chikamoto et al.*, 2015]. Our findings are further supported by *Dunstone et al.* [2011], where tropical Atlantic SSTs are shown to be forced from the subpolar gyre region and concluded to generate predictable low-frequency variability of the atmosphere in the tropical Atlantic [see, e.g., *Hawkins et al.*, 2011; *Msadek et al.*, 2014].

The Atlantic-Pacific lag-lead relationship with the AWT suggests that the synchronized atmospheric anomalies connecting the tropical Pacific to the Atlantic through the sub-Arctic are in the first place initiated by the NAO, which manifests itself as a tripole pattern (Figure 5). The Rossby wave flux from the tropical Pacific and toward the Atlantic is, however, not excited until the AWT changes phase and the transbasin variability is "activated" and is likely to feedback (e.g., through turbulent heat fluxes) on the subpolar region. It is thus important to consider this tropical-extratropical teleconnection of Pacific origin to better understand the anomalously warm and cold multiyears in the SPNA, where the AMO has its largest signal [*Ruiz-Barradas et al.*, 2013; *Buckley and Marshall*, 2016].

The decadal variability of AWT in the SPNA and its associated global linkages are shown here to be an essential aspect of the tropical interactions between the Atlantic and Pacific Oceans, with potential for improved decadal predictability [*Dunstone et al.*, 2011; *Chikamoto et al.*, 2015; *Keenlyside et al.*, 2015]. However, the mechanisms at play during the early 21st century decadal slowdown were rather pronounced as compared to those of the 1950s to the 1970s. This could be symptomatic of the sparse data record preceding the wide advent of expendable bathythermograph measurements in the mid-1970s. It could also suggest that global warming is amplifying the Atlantic and Pacific climate modes that enhance the appearance of transbasin linkages and feedbacks, particularly due to the relatively strong basin-wide warming of the tropical North Atlantic over the past two decades.

Acknowledgments

The authors wish to thank Thomas Rossby, Johan Nilsson, and the two anonymous reviewers for their insightful comments and helpful suggestions. L.C. is supported by the Jason Altimetry Program. S.H. is supported by the NASA Physical Oceanography Program. M.H.E. is supported by the Australian Research Council. S. N. and A. R.-B. gratefully acknowledge the support of the US National Science Foundation through grant AGS1439940. AWT data are included as a supporting information file; any additional data may be obtained from L.C. (leon.chafik@uib.no). This work was completed at the corresponding author's current affiliation (Geophysical Institute, University of Bergen, Norway).

References

Balmaseda, M. A., K. E. Trenberth, and E. Källén (2013), Distinctive climate signals in reanalysis of global ocean heat content, *Geophys. Res. Lett.*, *40*(9), 1754–1759.

Barrier, N., J. Deshayes, A.-M. Treguier, and C. Cassou (2015), Heat budget in the North Atlantic subpolar gyre: Impacts of atmospheric weather regimes on the 1995 warming event, *Prog. Oceanogr.*, *130*, 75–90.

Buckley, M. W., and J. Marshall (2016), Observations, inferences, and mechanisms of the Atlantic Meridional Overturning Circulation: A review, *Rev. Geophys.*, *54*(1), 5–63, doi:10.1002/2015RG000493.

Chafik, L., T. Rossby, and C. Schrum (2014), On the spatial structure and temporal variability of poleward transport between Scotland and Greenland, *J. Geophys. Res. Oceans*, *119*(2), 824–841, doi:10.1002/2013JC009287.

Chafik, L., J. Nilsson, Ø. Skagseth, and P. Lundberg (2015), On the flow of Atlantic water and temperature anomalies in the Nordic Seas toward the Arctic Ocean, *J. Geophys. Res. Oceans*, *120*, 7897–7918, doi:10.1002/2015JC011012.

Chen, X., and K.-K. Tung (2014), Varying planetary heat sink led to global-warming slowdown and acceleration, *Science*, *345*(6199), 897–903.

Chikamoto, Y., M. Kimoto, M. Watanabe, M. Ishii, and T. Mochizuki (2012), Relationship between the Pacific and Atlantic stepwise climate change during the 1990s, *Geophys. Res. Lett.*, *39*, L21710, doi:10.1029/2012GL053901.

Chikamoto, Y., A. Timmermann, J.-J. Luo, T. Mochizuki, M. Kimoto, M. Watanabe, M. Ishii, S.-P. Xie, and F.-F. Jin (2015), Skilful multi-year predictions of tropical trans-basin climate variability, *Nat. Commun.*, *6*, 6869, doi:10.1038/ncomms7869.

Compo, G. P., et al. (2011), The Twentieth Century Reanalysis project, *Q. J. R. Meteorolog. Soc.*, *137*(654), 1–28.

Czaja, A., and C. Frankignoul (1999), Influence of the North Atlantic SST on the atmospheric circulation, *Geophys. Res. Lett.*, *26*(19), 2969–2972.
Czaja, A., and C. Frankignoul (2002), Observed impact of Atlantic SST anomalies on the North Atlantic Oscillation, *J. Clim.*, *15*(6), 606–623.
Ding, Q., J. M. Wallace, D. S. Battisti, E. J. Steig, A. J. Gallant, H.-J. Kim, and L. Geng (2014), Tropical forcing of the recent rapid Arctic warming in northeastern Canada and Greenland, *Nature*, *509*(7499), 209–212.
Drews, A., and R. J. Greatbatch (2016), Atlantic multidecadal variability in a model with an improved North Atlantic Current, *Geophys. Res. Lett.*, *43*, 8199–8206, doi:10.1002/2016GL069815.
Drijfhout, S., A. Blaker, S. Josey, A. Nurser, B. Sinha, and M. Balmaseda (2014), Surface warming hiatus caused by increased heat uptake across multiple ocean basins, *Geophys. Res. Lett.*, *41*(22), 7868–7874.
Dunstone, N., D. Smith, and R. Eade (2011), Multi-year predictability of the tropical Atlantic atmosphere driven by the high latitude North Atlantic Ocean, *Geophys. Res. Lett.*, *38*, L14701, doi:10.1029/2011GL047949.
Ebisuzaki, W. (1997), A method to estimate the statistical significance of a correlation when the data are serially correlated, *J. Clim.*, *10*(9), 2147–2153.
Eden, C., and J. Willebrand (2001), Mechanism of interannual to decadal variability of the North Atlantic Circulation, *J. Clim.*, *14*(10), 2266–2280.
Enfield, D. B., A. M. Mestas-Nuñez, and P. J. Trimble (2001), The Atlantic Multidecadal Oscillation and its relation to rainfall and river flows in the continental us, *Geophys. Res. Lett.*, *28*(10), 2077–2080.
England, M. H., S. McGregor, P. Spence, G. A. Meehl, A. Timmermann, W. Cai, A. S. Gupta, M. J. McPhaden, A. Purich, and A. Santoso (2014), Recent intensification of wind-driven circulation in the Pacific and the ongoing warming hiatus, *Nat. Clim. Change*, *4*(3), 222–227.
Frankignoul, C., G. de Coëtlogon, T. M. Joyce, and S. Dong (2001), Gulf Stream variability and ocean-atmosphere interactions, *J. Phys. Oceanogr.*, *31*(12), 3516–3529.
Fyfe, J. C., et al. (2016), Making sense of the early-2000s warming slowdown, *Nat. Clim. Change*, *6*(3), 224–228.
Gastineau, G., and C. Frankignoul (2012), Cold-season atmospheric response to the natural variability of the Atlantic meridional overturning circulation, *Clim. Dyn.*, *39*(1–2), 37–57.
Gastineau, G., and C. Frankignoul (2015), Influence of the North Atlantic SST variability on the atmospheric circulation during the twentieth century, *J. Clim.*, *28*(4), 1396–1416.
Good, S. A., M. J. Martin, and N. A. Rayner (2013), EN4: Quality controlled ocean temperature and salinity profiles and monthly objective analyses with uncertainty estimates, *J. Geophys. Res. Oceans*, *118*(12), 6704–6716.
Grist, J. P., S. A. Josey, R. Marsh, S. A. Good, A. C. Coward, B. A. De Cuevas, S. G. Alderson, A. L. New, and G. Madec (2010), The roles of surface heat flux and ocean heat transport convergence in determining Atlantic Ocean temperature variability, *Ocean Dyn.*, *60*(4), 771–790.
Guan, B., and S. Nigam (2009), Analysis of Atlantic SST variability factoring interbasin links and the secular trend: Clarified structure of the Atlantic multidecadal oscillation, *J. Clim.*, *22*(15), 4228–4240.
Häkkinen, S., and P. B. Rhines (2004), Decline of subpolar North Atlantic circulation during the 1990s, *Science*, *304*(5670), 555–559.
Häkkinen, S., and P. B. Rhines (2009), Shifting surface currents in the northern North Atlantic Ocean, *J. Geophys. Res.*, *114*, C04005, doi:10.1029/2008JC004883.
Häkkinen, S., P. B. Rhines, and D. L. Worthen (2011a), Warm and saline events embedded in the meridional circulation of the northern North Atlantic, *J. Geophys. Res.*, *116*, C03006, doi:10.1029/2010JC006275.
Häkkinen, S., P. B. Rhines, and D. L. Worthen (2011b), Atmospheric blocking and Atlantic multidecadal ocean variability, *Science*, *334*(6056), 655–659.
Häkkinen, S., P. B. Rhines, and D. L. Worthen (2013), Northern North Atlantic sea surface height and ocean heat content variability, *J. Geophys. Res. Oceans*, *118*(7), 3670–3678.
Hamed, K. H., and A. R. Rao (1998), A modified Mann-Kendall trend test for autocorrelated data, *J. Hydrol.*, *204*(1), 182–196.
Hátún, H., A. Sandø, H. Drange, B. Hansen, and H. Valdimarsson (2005), Influence of the Atlantic subpolar gyre on the thermohaline circulation, *Science*, *309*(5742), 1841–1844.
Hawkins, E., J. Robson, R. Sutton, D. Smith, and N. Keenlyside (2011), Evaluating the potential for statistical decadal predictions of sea surface temperatures with a perfect model approach, *Clim. Dyn.*, *37*(11–12), 2495–2509.
Held, I. M. (2013), Climate science: The cause of the pause, *Nature*, *501*(7467), 318–319.
Herbaut, C., and M.-N. Houssais (2009), Response of the eastern North Atlantic subpolar gyre to the North Atlantic Oscillation, *Geophys. Res. Lett.*, *36*, L17607, doi:10.1029/2009GL039090.
Horel, J. D., and J. M. Wallace (1981), Planetary-scale atmospheric phenomena associated with the Southern Oscillation, *Mon. Weather Rev.*, *109*(4), 813–829.
Huang, B., P. W. Thorne, T. M. Smith, W. Liu, J. Lawrimore, V. F. Banzon, H.-M. Zhang, T. C. Peterson, and M. Menne (2016), Further exploring and quantifying uncertainties for Extended Reconstructed Sea Surface Temperature (ERSST) version 4 (v4), *J. Clim.*, *29*(9), 3119–3142.
Joyce, T. M., and R. Zhang (2010), On the path of the Gulf stream and the Atlantic meridional overturning circulation, *J. Clim.*, *23*(11), 3146–3154.
Katsman, C., and G. J. van Oldenborgh (2011), Tracing the upper ocean's "missing heat", *Geophys. Res. Lett.*, *38*, L14610, doi:10.1029/2011GL048417.
Keenlyside, N. S., J. Ba, J. Mecking, N.-E. Omrani, M. Latif, R. Zhang, and R. Msadek (2015), North Atlantic multi-decadal variability—Mechanisms and predictability, in *Climate Change Multidecadal Beyond*, edited by C.-P. Chang et al., pp. 141–158, World Scientific Publ., Singapore.
Knight, J. R., C. K. Folland, and A. A. Scaife (2006), Climate impacts of the Atlantic multidecadal oscillation, *Geophys. Res. Lett.*, *33*(17), L17706, doi:10.1029/2006GL026242.
Kosaka, Y., and S.-P. Xie (2013), Recent global-warming hiatus tied to equatorial Pacific surface cooling, *Nature*, *501*(7467), 403–407.
Kucharski, F., I.-S. Kang, R. Farneti, and L. Feudale (2011), Tropical Pacific response to 20th century Atlantic warming, *Geophys. Res. Lett.*, *38*(3), L03702, doi:10.1029/2010GL046248.
Kucharski, F., F. Ikram, F. Molteni, R. Farneti, I.-S. Kang, H.-H. No, M. P. King, G. Giuliani, and K. Mogensen (2015), Atlantic forcing of Pacific decadal variability, *Clim. Dyn.*, *46*, 2337–2351, doi:10.1007/s00382-015-2705-z.
Li, X., S.-P. Xie, S. T. Gille, and C. Yoo (2015), Atlantic-induced pan-tropical climate change over the past three decades, *Nat. Clim. Change*, *6*, 275–279, doi:10.1038/NCLIMATE2840.
Lindzen, R. S., and S. Nigam (1987), On the role of sea surface temperature gradients in forcing low-level winds and convergence in the tropics, *J. Atmos. Sci.*, *44*(17), 2418–2436.
Lohmann, K., H. Drange, and M. Bentsen (2009), A possible mechanism for the strong weakening of the North Atlantic subpolar gyre in the mid-1990s, *Geophys. Res. Lett.*, *36*, L15602, doi:10.1029/2009GL039166.

Lozier, M. S., S. Leadbetter, R. G. Williams, V. Roussenov, M. S. Reed, and N. J. Moore (2008), The spatial pattern and mechanisms of heat-content change in the North Atlantic, *Science*, *319*(5864), 800–803.
Lozier, M. S., V. Roussenov, M. S. Reed, and R. G. Williams (2010), Opposing decadal changes for the North Atlantic meridional overturning circulation, *Nat. Geosci.*, *3*(10), 728–734.
Maher, N., A. S. Gupta, and M. H. England (2014), Drivers of decadal hiatus periods in the 20th and 21st centuries, *Geophys. Res. Lett.*, *41*(16), 5978–5986, doi:10.1002/2014GL060527.
Mantua, N. J. (1997), A Pacific interdecadal climate oscillation with impacts on salmon production, *Bull. Am. Meteorol. Soc.*, *78*, 1069–1079.
Marshall, J., H. Johnson, and J. Goodman (2001), A study of the interaction of the North Atlantic Oscillation with ocean circulation, *J. Clim.*, *14*(7), 1399–1421.
McCarthy, G. D., I. D. Haigh, J. J.-M. Hirschi, J. P. Grist, and D. A. Smeed (2015), Ocean impact on decadal Atlantic climate variability revealed by sea-level observations, *Nature*, *521*(7553), 508–510.
McGregor, S., A. Timmermann, M. F. Stuecker, M. H. England, M. Merrifield, F.-F. Jin, and Y. Chikamoto (2014), Recent Walker circulation strengthening and Pacific cooling amplified by Atlantic warming, *Nat. Clim. Change*, *4*(10), 888–892.
Meehl, G. A., J. M. Arblaster, J. T. Fasullo, A. Hu, and K. E. Trenberth (2011), Model-based evidence of deep-ocean heat uptake during surface-temperature hiatus periods, *Nat. Clim. Change*, *1*(7), 360–364.
Msadek, R., et al. (2014), Predicting a decadal shift in North Atlantic climate variability using the GFDL forecast system, *J. Clim.*, *27*(17), 6472–6496.
Peings, Y., and G. Magnusdottir (2014), Forcing of the wintertime atmospheric circulation by the multidecadal fluctuations of the North Atlantic Ocean, *Environ. Res. Lett.*, *9*(3), 034018.
Reverdin, G. (2010), North Atlantic subpolar gyre surface variability (1895–2009), *J. Clim.*, *23*(17), 4571–4584.
Robson, J., R. Sutton, K. Lohmann, D. Smith, and M. D. Palmer (2012), Causes of the rapid warming of the North Atlantic Ocean in the mid-1990s, *J. Clim.*, *25*(12), 4116–4134.
Robson, J., P. Ortega, and R. Sutton (2016), A reversal of climatic trends in the North Atlantic since 2005, *Nat. Geosci.*, *9*(7), 513–517.
Rossby, T., and R. Benway (2000), Slow variations in mean path of the Gulf Stream east of Cape Hatteras, *Geophys. Res. Lett.*, *27*(1), 117–120.
Ruiz-Barradas, A., S. Nigam, and A. Kavvada (2013), The Atlantic Multidecadal Oscillation in twentieth century climate simulations: Uneven progress from CMIP3 to CMIP5, *Clim. Dyn.*, *41*(11–12), 3301–3315.
Song, Y., Y. Yu, and P. Lin (2014), The hiatus and accelerated warming decades in CMIP5 simulations, *Adv. Atmos. Sci.*, *31*(6), 1316–1330.
Steinman, B. A., M. E. Mann, and S. K. Miller (2015), Atlantic and Pacific multidecadal oscillations and Northern Hemisphere temperatures, *Science*, *347*(6225), 988–991.
Stocker, T., D. Qin, G. Plattner, M. Tignor, S. Allen, J. Boschung, A. Nauels, Y. Xia, B. Bex, and B. Midgley (2013), *IPCC, 2013: Climate Change 2013—The Physical Science Basis. Contribution of Working Group I to the Fifth Assessment Report of the Intergovernmental Panel on Climate Change*, 1535 pp., Cambridge Univ. Press, Cambridge, U. K., and New York.
Timmermann, A., et al. (2007), The influence of a weakening of the Atlantic meridional overturning circulation on ENSO, *J. Clim.*, *20*(19), 4899–4919.
Trenberth, K. E. (2015), Has there been a hiatus, *Science*, *349*(6249), 691.
Trenberth, K. E., and J. T. Fasullo (2013), An apparent hiatus in global warming?, *Earth's Future*, *1*(1), 19–32, doi:10.1002/2013EF000165.
Trenberth, K. E, G. W. Branstator, D. Karoly, A. Kumar, N.-C. Lau, and C. Ropelewski (1998), Progress during TOGA in understanding and modeling global teleconnections associated with tropical sea surface temperatures, *J. Geophys. Res.*, *103*(C7), 14,291–14,324.
Trenberth, K. E., J. T. Fasullo, G. Branstator, and A. S. Phillips (2014), Seasonal aspects of the recent pause in surface warming, *Nat. Clim. Change*, *4*(10), 911–916.
Von Storch, H., and F. W. Zwiers (2001), *Statistical analysis in climate research*, Cambridge Univ. Press, Cambridge, U. K.
Wang, C. (2006), An overlooked feature of tropical climate: Inter-Pacific-Atlantic variability, *Geophys. Res. Lett.*, *33*, L12702, doi:10.1029/2006GL026324.
Watanabe, M., H. Shiogama, H. Tatebe, M. Hayashi, M. Ishii, and M. Kimoto (2014), Contribution of natural decadal variability to global warming acceleration and hiatus, *Nat. Clim. Change*, *4*(10), 893–897.
Wouters, B., S. Drijfhout, and W. Hazeleger (2012), Interdecadal North-Atlantic meridional overturning circulation variability in EC-EARTH, *Clim. Dyn.*, *39*(11), 2695–2712.
Yeager, S., A. Karspeck, G. Danabasoglu, J. Tribbia, and H. Teng (2012), A decadal prediction case study: Late twentieth-century North Atlantic Ocean heat content, *J. Clim.*, *25*(15), 5173–5189.
Zhang, R. (2008), Coherent surface-subsurface fingerprint of the Atlantic meridional overturning circulation, *Geophys. Res. Lett.*, *35*(20), L20705, doi:10.1029/2008GL035463.
Zhang, R., R. Sutton, G. Danabasoglu, T. L. Delworth, W. M. Kim, J. Robson, and S. G. Yeager (2016), Comment on "the Atlantic Multidecadal Oscillation without a role for ocean circulation", *Science*, *352*(6293), 1527–1527.

Supporting Information for "Global Linkages Originating from Decadal Oceanic Variability in the Subpolar North Atlantic"

L. Chafik[1,2], S. Häkkinen[3], M. H. England[4], J. A. Carton[5], S. Nigam[5], A. Ruiz-Barradas[5], A. Hannachi[6], L. Miller[1]

[1]NOAA/NESDIS Center for Satellite Application and Research, College Park, MD, USA

[2]Cooperative Institute for Climate and Satellites, University of Maryland, College Park, MD, USA

[3]NASA Goddard Space Flight Center, Greenbelt, Maryland, USA.

[4]Australian Research Council Centre of Excellence for Climate System Science and Climate Change Research Centre, University of New South Wales, Sydney, New South Wales, Australia

Contents of this file

1. Text S1 to S10

2. Figures S1 to S10

Introduction

Text S1. Figure S1 is based on NOAA ERSSTv4 data [*Huang et al.*, 2016], and it shows the averaged global air temperature deviations from the 1971-2000 climatology. The 1950-1970s and 2001-2012 hiatuses are clear and co-vary with the warm periods in the SPNA. While between these two periods, acceleration in global warming is evident and coincide with anomalously cold SPNA period.

Text S2. Figure S2 shows the raw Atlantic Water subsurface temperature variability index before removing the seasonal cycle and the linear trend. This subsurface index is within Atlantic Water in the Subpolar North Atlantic and co-located with the core of the North Atlantic Current. The low-frequency variability of our index bears similarity to the Atlantic Multidecadal Oscillation (AMO), however, we have chosen not to use the AMO index. This is because our objective is to explore how the SPNA (where the AMO actually has its largest loading, see e.g. *Ruiz-Barradas et al.* [2013]) decadal variability

[5]Department of Atmospheric and Oceanic

Science, University of Maryland, College

Park, Maryland, USA

[6]Department of Meteorology, Stockholm

University, Stockholm, Sweden

may be set, but most importantly, its potential role in influencing the Pacific decadal variability. Furthermore, we note that our index resembles the spatial pattern of the second empirical orthogonal function mode of North Atlantic ocean heat *Häkkinen et al.* [2013], which suggests that the AWT index does not suffer from being locally constructed. Interestingly, the regime transitions of the AWT appear to resemble those associated with the Atlantic meridional overturning circulation (calculated at 45°N) reported in multi-system forecast models [*Pohlmann et al.*, 2013].

Text S3. Figure S3 shows the 1949-2013 progression of ocean heat content anomalies. This suggest that heat anomalies initially appear in the Gulf Stream region along its path, before they are advected along the Gulf Stream and North Atlantic Current pathway towards the eastern subpolar gyre and around the Labrador Sea. Note that the decadal variability is strongly confined to the Gulf Stream region and Subpolar gyre region [*Zhang*, 2008]. The decadal evolution of heat content into the SPNA is largely driven by ocean heat transport convergence [*Grist et al.*, 2010] as a response to the NAO through excursions in the subtropical-subpolar boundary [*Marshall et al.*, 2001; *McCarthy et al.*, 2015]. Furthermore, enhanced northward penetration of Gulf Stream waters into the subpolar regions has, in both observations and tracer experiments, been found to be induced by horizontal changes in the gyre circulation as a response to low-frequency wind-stress curl variability [*Häkkinen and Rhines*, 2009; *Häkkinen et al.*, 2011a, 2013].

Text S4. Figure S4 shows the spatial pattern of wind-stress curl of the second EOF mode and its associated principal component. The variability of the latter reflects the strength of the gyres. Warm and saline periods in the northern North Atlantic are related

to weaker wind stress curl phase and a westward shift of the polar front. The tilt of the isopycnals in both gyres decreases during the weak phase leading to a contraction the subpolar gyre and expansion of the subtropical gyre allowing warm and saline subtropical waters to advect into the subpolar gyre region [*Häkkinen et al.*, 2011a, b, 2013], thereby contributing to the decadal-scale variability of AWT.

Text S5-S6. Sliding 7-year time-windows of SSTs (Fig. S5) and 200-hPa (Fig. S6) geopotential height anomalies (non-zonal) for the 1950-2011 period. We note that positive SST anomalies coincide well with positive geopotential height anomalies. For example, the tripole SST pattern in the North Atlantic due to the NAO can also be seen in the geopotential height at 200-hPa. Note also that the warm (cold) periods of the North Atlantic coincide with a negative (positive) PDO pattern. The wave-like features emanating from the tropical Pacific are particularly pronounced during negative PDO (Fig. 4) and connect to the Atlantic following a great circle route (e.g. *Hoskins and Karoly* [1981]).

Text S7-S8. Inter-comparison between indices of the AWT and the AMO show some similarities but differences are also clear (Fig. S7 and S8). The indices are simultaneously correlated (0.37 and 0.64 when raw and smoothed with a 25-month running mean, respectively), however, maximum correlation is shown when AMO leads by 2 years (r=0.68). However, we admit that it is difficult to judge these correlations since they are similar in the window ranging between -2 and +2 years.

We also note that AWT has a shorter damping timescale than the AMO; SST anomalies regressed onto AWT change sign in a lapse of 10 years while those based on the AMO index remain on the same sign for a longer period (Fig. S8). We think that AWT may

be representative of the subpolar part of the Atlantic multidecadal variability, but it is difficult to separate it from its tropical part, as anomalies in the SPNA later connect with the tropics. Regressions in Fig. S12 suggest that SST anomalies related to both indices move eastward with time and reach the tropics following the subpolar gyre completing the horse-shoe pattern. The propagation and intensification of surface temperature anomalies toward the tropics setting the horse-shoe pattern is, however, not a minor issue since both ocean heat convergence and surface fluxes have there been shown to be equally important [*Grist et al.*, 2010]. In addition, a recent study by *Brown et al.* [2016] pointed out that cloud feedback may be a necessary mechanism for the tropical portion of the AMO. The ocean circulation and especially that associated with the SPNA plays an important role in driving this coherent decadal North Atlantic climate variability, as recently pointed out by *Zhang et al.* [2016] (see also *Drews and Greatbatch* [2016]).

Text S9. Figure S9 shows the decadal Pacific variability and the extended AWT index. It also shows the lag-correlation between AWT and NAO, PDO and western tropical Pacific surface wind anomalies. Note that the NAO leads the AWT by about 6-18 months (maximum correlation at 12 months), while the PDO and western tropical Pacific surface winds lag the AWT both by about 2-3 years (maximum correlation at 31 months). The NAO encourages phase reversal of the decadal variability in AWT, which in turn, leads the western Pacific trade winds and Pacific decadal variability. Note, for example, that the 1995 subpolar gyre warming lasted for a period of 17 years. The reversal in the northern North Atlantic, according to AWT, started at the end 2012. While, the PDO reversed in 2015. *Robson et al.* [2016] recently suggested that this reversal in the North

Atlantic climate since 2005 (note the trend in Fig. S8b) has been induced by low density anomalies in the Labrador Sea during the warming of the past decade, which in turn led to a slowdown of the meridional overturning circulation and northward heat transport. Taken together, these results suggest that the Atlantic decadal climate variability may be leading that of the Pacific, which is in line with Fig. 5, and results reported by *Chikamoto et al.* [2012].

Text S10. Figure S10a demonstrates the fact that the large-scale trans-basin variability also reflects the strength of the trade winds as averaged in the western tropical Pacific (160°-180°E, 5°S-5°N), both on monthly and decadal timescales (Figure S10b). The large-scale trans-basin variability, following *McGregor et al.* [2014], is seen on longer timescales to co-vary with the phases of AWT. The simultaneous and correlation between trans-basin variability and AWT are 0.5 and 0.62, respectively. Fig. S10c also indicate that AWT index is leading that of trans-basin variability by about 21 months.

References

Brown, P. T., M. S. Lozier, R. Zhang, and W. Li (2016), The necessity of cloud feedback for a basin-scale Atlantic Multidecadal Oscillation, *Geophysical Research Letters*, *43*(8), 3955–3963.

Chikamoto, Y., M. Kimoto, M. Watanabe, M. Ishii, and T. Mochizuki (2012), Relationship between the Pacific and Atlantic stepwise climate change during the 1990s, *Geophysical Research Letters*, *39*(21).

Drews, A., and R. J. Greatbatch (2016), Atlantic Multidecadal variability in a model with an improved North Atlantic Current, *Geophysical Research Letters*.

Ebisuzaki, W. (1997), A method to estimate the statistical significance of a correlation when the data are serially correlated, *Journal of Climate*, *10*(9), 2147–2153.

Grist, J. P., S. A. Josey, R. Marsh, S. A. Good, A. C. Coward, B. A. De Cuevas, S. G. Alderson, A. L. New, and G. Madec (2010), The roles of surface heat flux and ocean heat transport convergence in determining Atlantic Ocean temperature variability, *Ocean dynamics*, *60*(4), 771–790.

Häkkinen, S., and P. B. Rhines (2009), Shifting surface currents in the northern North Atlantic Ocean, *Journal of Geophysical Research: Oceans*, *114*(C4), n/a–n/a, doi: 10.1029/2008JC004883.

Häkkinen, S., P. B. Rhines, and D. L. Worthen (2011a), Warm and saline events embedded in the meridional circulation of the northern North Atlantic, *Journal of Geophysical Research: Oceans*, *116*(C3).

Häkkinen, S., P. B. Rhines, and D. L. Worthen (2011b), Atmospheric blocking and Atlantic multidecadal ocean variability, *Science*, *334*(6056), 655–659.

Häkkinen, S., P. B. Rhines, and D. L. Worthen (2013), Northern North Atlantic sea surface height and ocean heat content variability, *Journal of Geophysical Research: Oceans*, *118*(7), 3670–3678.

Hoskins, B. J., and D. J. Karoly (1981), The steady linear response of a spherical atmosphere to thermal and orographic forcing, *Journal of the Atmospheric Sciences*, *38*(6), 1179–1196.

Huang, B., P. W. Thorne, T. M. Smith, W. Liu, J. Lawrimore, V. F. Banzon, H.-M. Zhang, T. C. Peterson, and M. Menne (2016), Further exploring and quantifying uncertainties

for Extended Reconstructed Sea Surface Temperature (ERSST) version 4 (v4), *Journal of Climate*, *29*(9), 3119–3142.

Marshall, J., H. Johnson, and J. Goodman (2001), A study of the interaction of the north atlantic oscillation with ocean circulation, *Journal of Climate*, *14*(7), 1399–1421.

McCarthy, G. D., I. D. Haigh, J. J.-M. Hirschi, J. P. Grist, and D. A. Smeed (2015), Ocean impact on decadal Atlantic climate variability revealed by sea-level observations, *Nature*, *521*(7553), 508–510.

McGregor, S., A. Timmermann, M. F. Stuecker, M. H. England, M. Merrifield, F.-F. Jin, and Y. Chikamoto (2014), Recent Walker circulation strengthening and Pacific cooling amplified by Atlantic warming, *Nature Climate Change*, *4*(10), 888–892.

Pohlmann, H., D. M. Smith, M. A. Balmaseda, N. S. Keenlyside, S. Masina, D. Matei, W. A. Müller, and P. Rogel (2013), Predictability of the mid-latitude Atlantic meridional overturning circulation in a multi-model system, *Climate dynamics*, *41*(3-4), 775–785.

Robson, J., P. Ortega, and R. Sutton (2016), A reversal of climatic trends in the North Atlantic since 2005, *Nature Geoscience*.

Ruiz-Barradas, A., S. Nigam, and A. Kavvada (2013), The Atlantic Multidecadal Oscillation in twentieth century climate simulations: uneven progress from CMIP3 to CMIP5, *Climate dynamics*, *41*(11-12), 3301–3315.

Zhang, R. (2008), Coherent surface-subsurface fingerprint of the Atlantic meridional overturning circulation, *Geophysical Research Letters*, *35*(20).

Zhang, R., R. Sutton, G. Danabasoglu, T. L. Delworth, W. M. Kim, J. Robson, and S. G. Yeager (2016), Comment on "the Atlantic Multidecadal Oscillation without a role for

ocean circulation", *Science*, *352*(6293), 1527–1527.

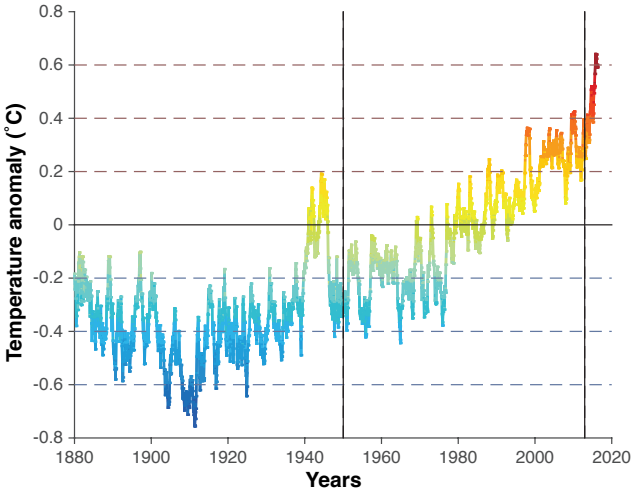

Figure S1. Global mean temperature anomaly from 1880 to 2015 (°C). The anomalies are deviations from the 1971-2000 climatology. The vertical black lines indicate the period under investigation in the present study.

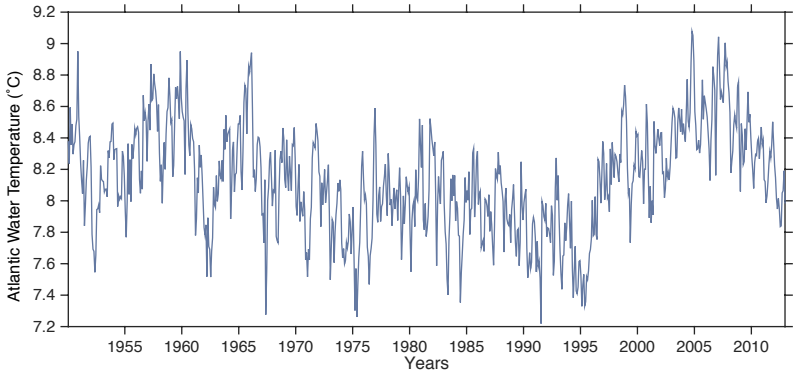

Figure S2. The raw monthly AWT variability (°C) between 1950 and 2012. It has a time-mean of 8.1 °C with a standard deviation of .3 °C.

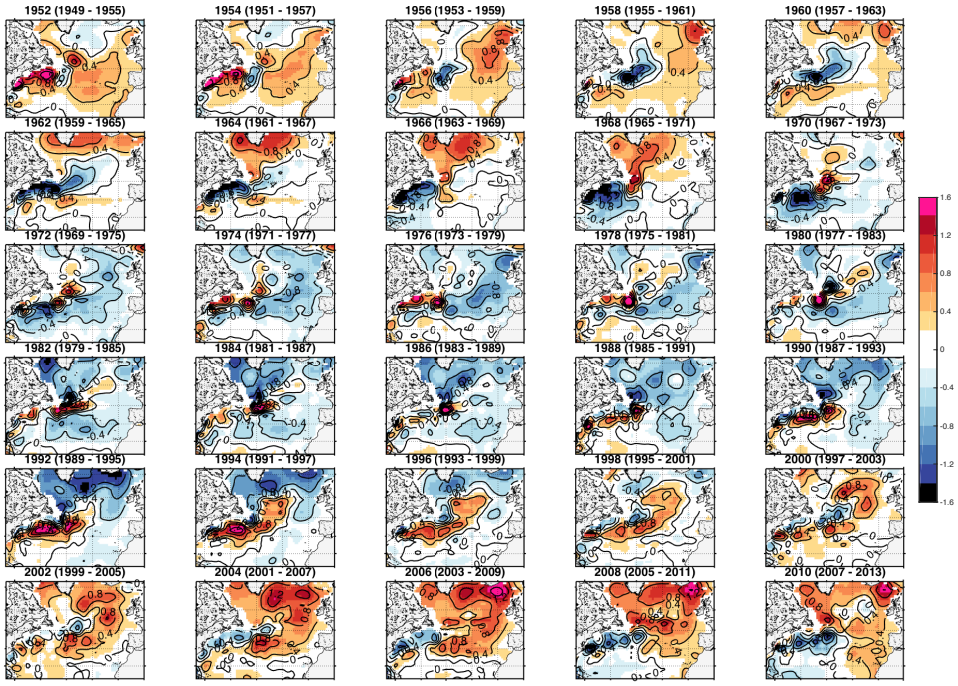

Figure S3. Sliding 7-year averages of ocean heat content anomalies (J m^{-2} x 10^9) during the 1949-2013 period.

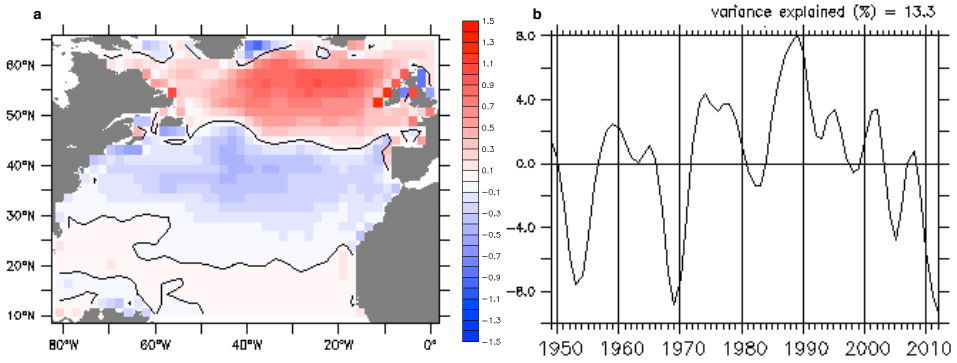

Figure S4. (a) The spatial pattern of the second empirical orthogonal function of the normalized DJFM wind stress curl, and (b) its principal component.

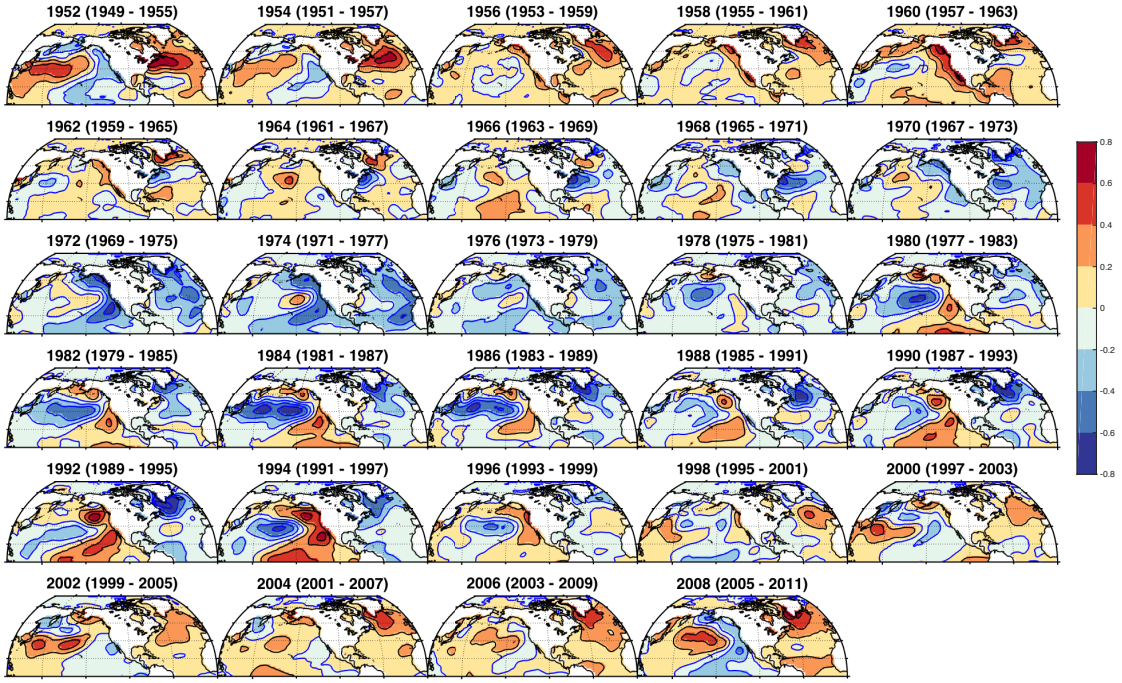

Figure S5. Sliding 7-year averages of Atlantic and Pacific SST anomalies (°C) during the 1949-2011 period.

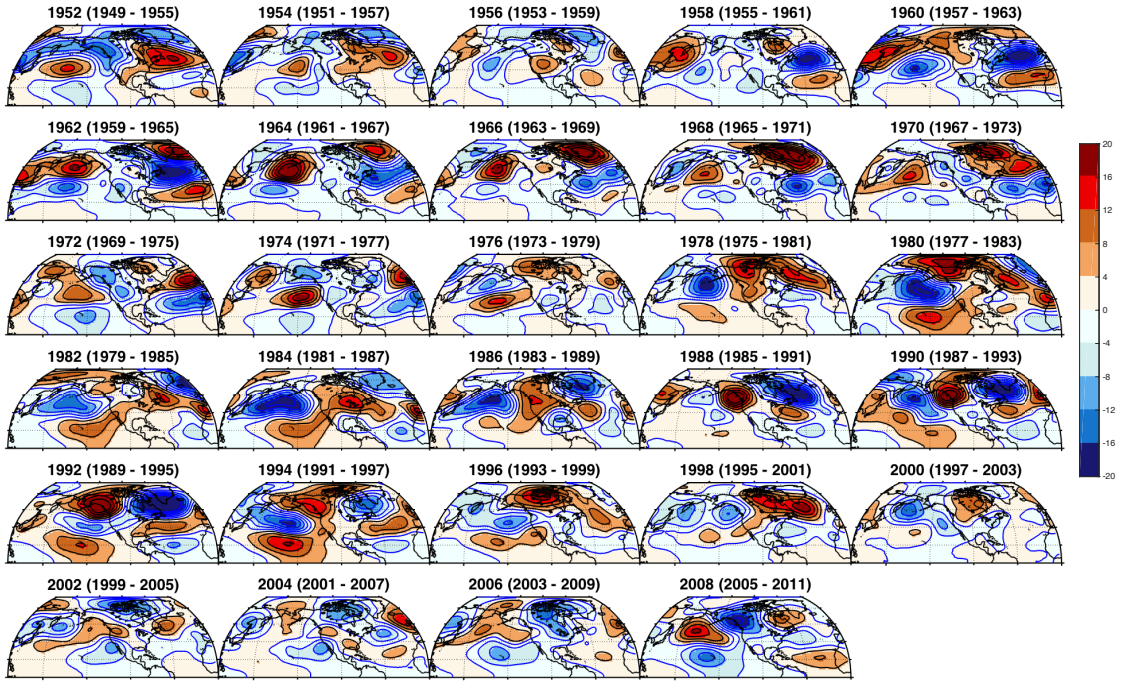

Figure S6. Sliding 7-year averages of Atlantic and Pacific geopotential height anomalies at 200-hPa (gpm) during the 1949-2011 period.

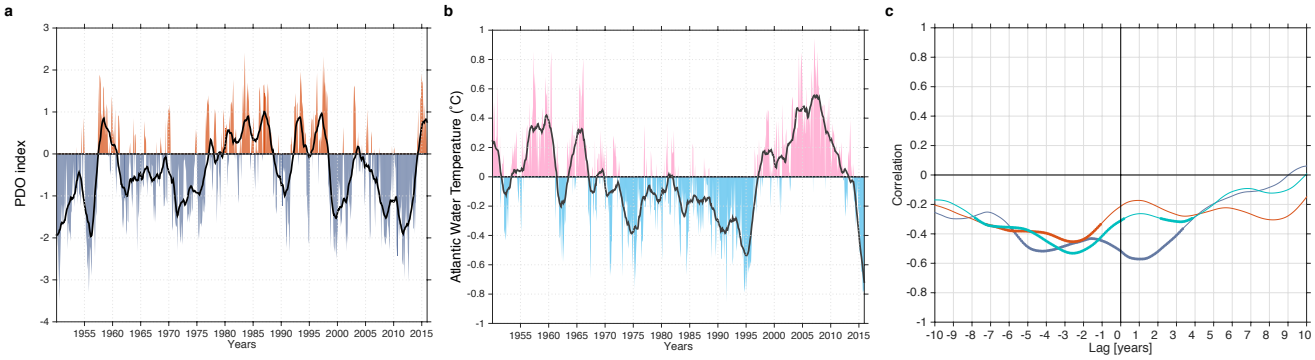

Figure S7. (a) The leading mode of decadal SST variability in the Pacific, i.e. the PDO. (b) The AWT extended until 2015, where the shading represents the raw monthly AWT (°C). The black lines in (a) and (b) indicate their smoothed versions using a 25-month running mean. Note the strong cooling since 2012. In comparison, the PDO changed phase in 2015 (see Fig. S9), a couple of years after a phase change in AWT. (c) Cross-correlation between AWT and NAO (blue), PDO (orange) and western tropical Pacific trade winds (turquoise). It is clear that the NAO leads AWT, while the PDO and the strength of the Walker circulation lag SPNA climate variability. Thicker line represents significant lag correlations at the 99% confidence level using 5000 Monte Carlo simulations, after *Ebisuzaki* [1997]. The smoothed AWT index is provided with the supplementary materials.

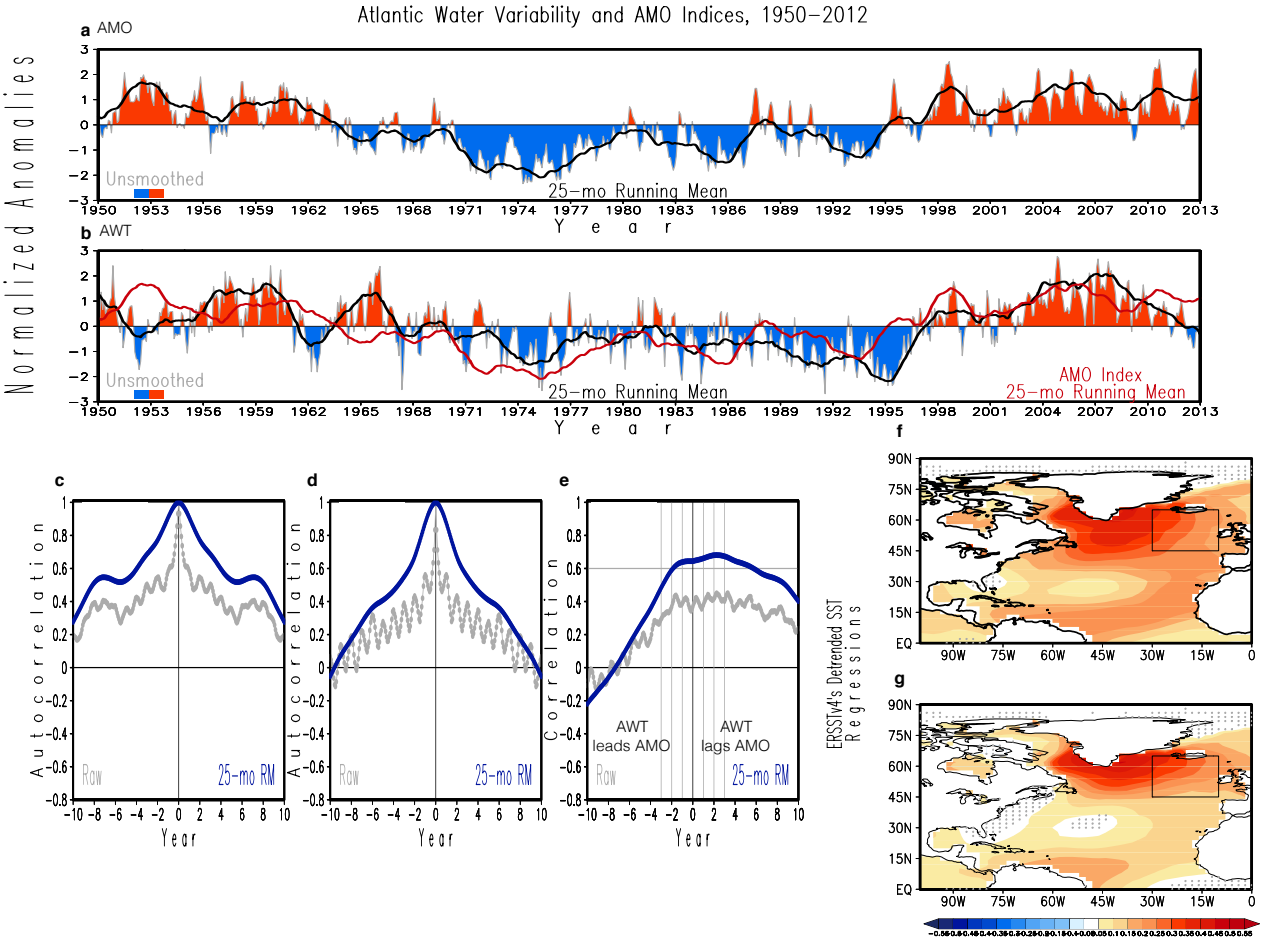

Figure S8. (a) Monthly and smoothed AMO index (25-month running mean), (b) AWT overlaid by the smoothed AMO index. Autocorrelation of the monthly (gray) and smoothed (c) AMO, (d) AWT indices. (e) Lag-correlation between AMO and AWT. Spatial regression of SST anomalies (°C) onto (f) AMO and (g) AWT. The black box shows approximate location of our AWT index. The gray stipplings indicate non-significance at the 99% confidence level.

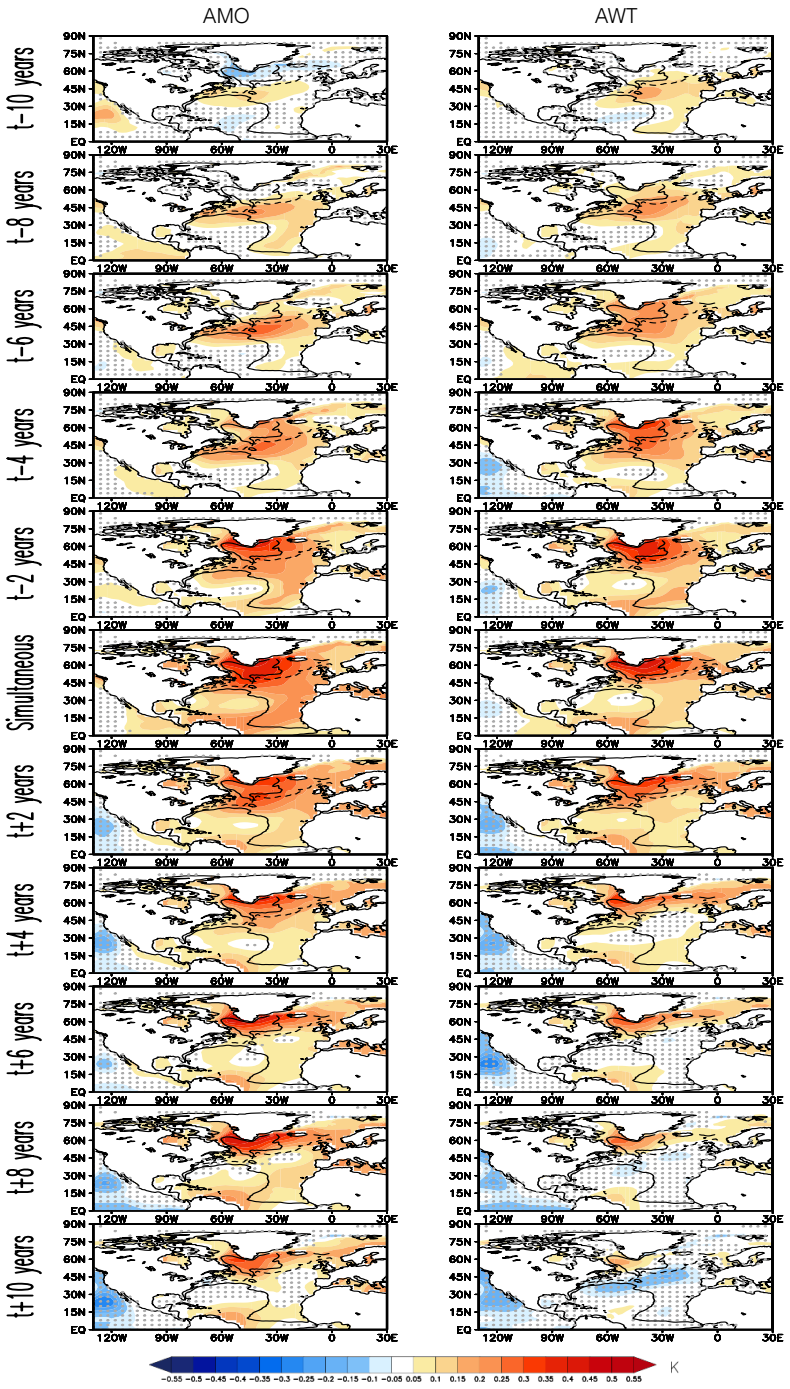

Figure S9. Spatial lag-regressions of SST anomalies (°C) onto (left) AMO and (right) AWT. The gray stipplings indicate non-significance at the 99% confidence level. The dashed black contour is the -.1 m isoline derived from time-mean absolute dynamic topography and separates the subpolar from the subtropical region (solid black contours).

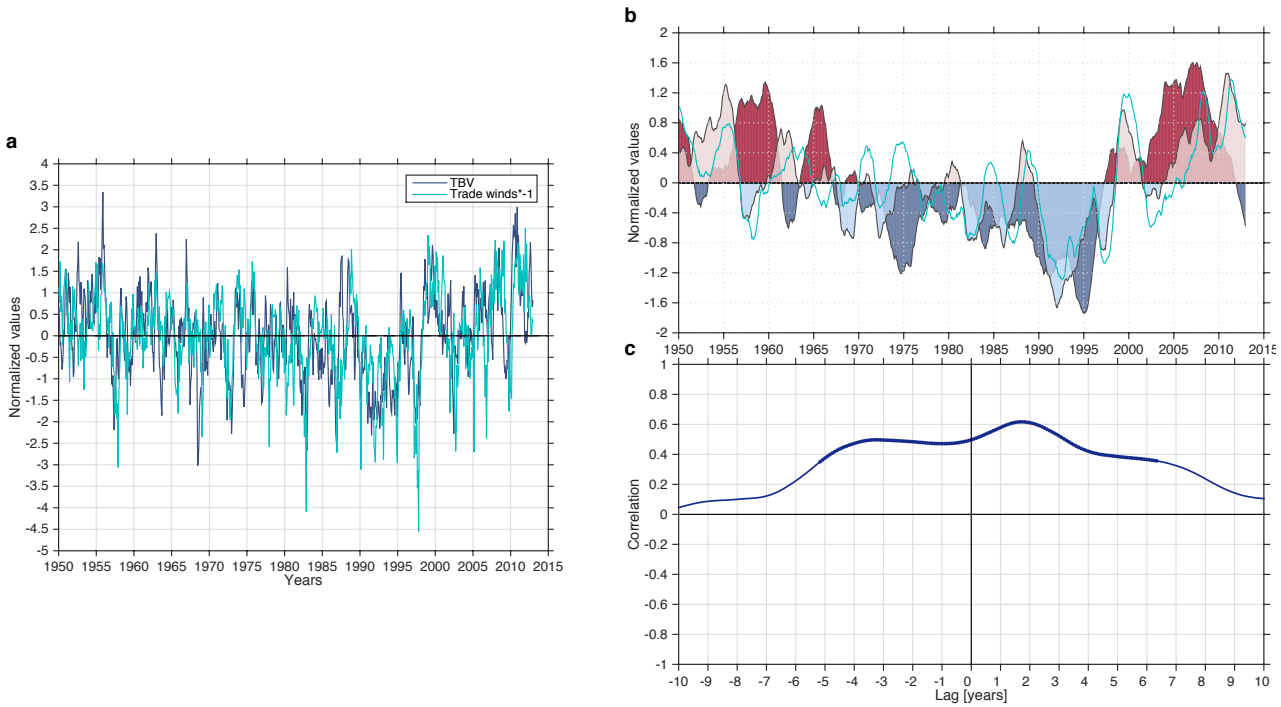

Figure S10. (a) Comparison between trans-basin variability (TBV, i.e. difference between Atlantic and Pacific SSTs (°C) [*McGregor et al.*, 2014] and western tropical Pacific trade winds (ms^{-1}). (b) Smoothed AWT (dark shading, in °C) overlaid by the smoothed trans-basin variability (light shading, in °C). The turquoise line represent the smoothed western tropical Pacific trade winds (ms^{-1}). (c) Cross-correlation between AWT and trans-basin variability. The former leads the latter by 21 months.

Smooth AWT variability index from 1950/01 until 2012/12, i.e. 756 data points.
The raw time series has been deseaonalized, linearly detrended and smoothed with a 25-month running mean.
0.2722
0.2684
0.2627
0.2561
0.2597
0.2440
0.2311
0.2222
0.2155
0.2116
0.2072
0.2054
0.1989
0.1771
0.1577
0.1235
0.0928
0.0567
0.0401
0.0214
0.0039
-0.0213
-0.0351
-0.0652
-0.0785
-0.0879
-0.0928
-0.0925
-0.0897
-0.1018
-0.0851
-0.0753
-0.0671
-0.0639
-0.0610
-0.0550
-0.0578
-0.0516
-0.0275
0.0005
0.0136
0.0304
0.0421
0.0430
0.0442
0.0548
0.0672
0.0670
0.0621
0.0495
0.0466

0.0613
0.0617
0.0665
0.0629
0.0621
0.0604
0.0560
0.0573
0.0570
0.0587
0.0688
0.0756
0.0703
0.0606
0.0670
0.0662
0.0904
0.1083
0.1271
0.1328
0.1340
0.1513
0.1801
0.2097
0.2473
0.2600
0.2816
0.3010
0.3285
0.3407
0.3516
0.3537
0.3622
0.3607
0.3489
0.3416
0.3260
0.3314
0.3417
0.3396
0.3513
0.3457
0.3459
0.3528
0.3615
0.3745
0.3763
0.3601
0.3536
0.3401
0.3408
0.3383
0.3327
0.3274

0.3172
0.3285
0.3395
0.3408
0.3516
0.3694
0.3694
0.4002
0.4241
0.4292
0.4330
0.4260
0.4196
0.4123
0.3992
0.3907
0.3805
0.3534
0.3452
0.3439
0.3235
0.3063
0.2866
0.2677
0.2451
0.2221
0.1798
0.1479
0.1208
0.0826
0.0604
0.0438
0.0002
-0.0574
-0.0950
-0.1200
-0.1311
-0.1533
-0.1709
-0.1772
-0.1907
-0.1945
-0.1731
-0.1604
-0.1634
-0.1575
-0.1691
-0.1609
-0.1626
-0.1491
-0.1315
-0.1048
-0.0767
-0.0500

-0.0328
-0.0239
-0.0021
0.0228
0.0421
0.0602
0.0736
0.0827
0.1055
0.1298
0.1469
0.1567
0.1601
0.1642
0.1801
0.2014
0.2173
0.2280
0.2349
0.2540
0.2674
0.2908
0.3133
0.3214
0.3115
0.3258
0.3225
0.3127
0.3097
0.3222
0.3283
0.3330
0.3293
0.3093
0.2882
0.2581
0.2586
0.2286
0.1952
0.1678
0.1394
0.1196
0.1119
0.0876
0.0545
0.0275
-0.0038
-0.0262
-0.0561
-0.0705
-0.0919
-0.0942
-0.0917
-0.0948

-0.1044
-0.1038
-0.0992
-0.0991
-0.0905
-0.0693
-0.0494
-0.0505
-0.0129
 0.0099
 0.0101
 0.0196
 0.0203
 0.0247
 0.0319
 0.0349
 0.0303
 0.0340
 0.0328
 0.0383
 0.0454
 0.0513
 0.0425
 0.0330
 0.0151
-0.0116
-0.0409
-0.0731
-0.0891
-0.1050
-0.1226
-0.1294
-0.1238
-0.1228
-0.1182
-0.1087
-0.1065
-0.1047
-0.1057
-0.1060
-0.0966
-0.0971
-0.0937
-0.1022
-0.0967
-0.0909
-0.0914
-0.0868
-0.0871
-0.0776
-0.0633
-0.0671
-0.0580
-0.0481

-0.0361
-0.0456
-0.0546
-0.0714
-0.0893
-0.1004
-0.1145
-0.1308
-0.1432
-0.1661
-0.1862
-0.2023
-0.2092
-0.2273
-0.2396
-0.2570
-0.2776
-0.2819
-0.2925
-0.3131
-0.3273
-0.3227
-0.3155
-0.3291
-0.3392
-0.3615
-0.3699
-0.3788
-0.3883
-0.3908
-0.3896
-0.3813
-0.3787
-0.3782
-0.3643
-0.3481
-0.3452
-0.3416
-0.3505
-0.3563
-0.3587
-0.3594
-0.3589
-0.3394
-0.2999
-0.2752
-0.2752
-0.2637
-0.2318
-0.2094
-0.1878
-0.1704
-0.1591
-0.1461

-0.1413
-0.1427
-0.1516
-0.1578
-0.1443
-0.1364
-0.1343
-0.1205
-0.1154
-0.0980
-0.0831
-0.0746
-0.0671
-0.0665
-0.0852
-0.1032
-0.1072
-0.1002
-0.1072
-0.1153
-0.1203
-0.1234
-0.1251
-0.1196
-0.1226
-0.1285
-0.1319
-0.1382
-0.1507
-0.1654
-0.1712
-0.1684
-0.1781
-0.1663
-0.1665
-0.1712
-0.1662
-0.1483
-0.1346
-0.1180
-0.0995
-0.1105
-0.1167
-0.1007
-0.1042
-0.1151
-0.1156
-0.1135
-0.1018
-0.0891
-0.0734
-0.0603
-0.0391
-0.0037

0.0052
-0.0084
-0.0122
-0.0019
-0.0101
-0.0131
-0.0059
-0.0028
-0.0086
-0.0208
-0.0354
-0.0633
-0.0759
-0.0908
-0.1028
-0.0999
-0.0895
-0.0869
-0.0862
-0.1078
-0.1174
-0.1351
-0.1471
-0.1580
-0.1793
-0.1880
-0.2001
-0.2197
-0.2418
-0.2537
-0.2609
-0.2672
-0.2764
-0.2833
-0.2803
-0.2627
-0.2579
-0.2384
-0.2191
-0.1994
-0.1847
-0.1958
-0.1976
-0.1957
-0.1819
-0.1862
-0.1777
-0.1727
-0.1803
-0.1809
-0.1848
-0.1742
-0.1578
-0.1456

-0.1416
-0.1426
-0.1445
-0.1488
-0.1524
-0.1562
-0.1727
-0.1788
-0.1855
-0.1779
-0.1860
-0.1952
-0.1818
-0.1784
-0.1775
-0.1824
-0.1773
-0.1767
-0.1898
-0.1761
-0.1645
-0.1614
-0.1567
-0.1649
-0.1716
-0.1830
-0.1788
-0.1769
-0.1632
-0.1612
-0.1633
-0.1643
-0.1582
-0.1615
-0.1886
-0.2070
-0.2056
-0.2211
-0.2304
-0.2367
-0.2381
-0.2352
-0.2446
-0.2494
-0.2688
-0.2877
-0.3027
-0.3140
-0.3167
-0.3194
-0.3116
-0.3158
-0.3326
-0.3447

-0.3559
-0.3590
-0.3673
-0.3934
-0.3887
-0.3748
-0.3715
-0.3883
-0.3854
-0.3866
-0.3912
-0.3974
-0.4065
-0.4035
-0.3879
-0.3773
-0.3854
-0.3850
-0.3693
-0.3545
-0.3477
-0.3329
-0.3259
-0.3183
-0.3242
-0.3282
-0.3296
-0.3261
-0.3028
-0.3143
-0.3231
-0.3221
-0.3129
-0.3144
-0.3155
-0.3063
-0.3142
-0.3286
-0.3383
-0.3510
-0.3726
-0.3787
-0.3884
-0.4089
-0.4326
-0.4488
-0.4803
-0.4951
-0.4986
-0.5050
-0.5109
-0.5186
-0.5272
-0.5408

-0.5471
-0.5546
-0.5608
-0.5594
-0.5614
-0.5555
-0.5519
-0.5414
-0.5293
-0.5036
-0.4844
-0.4572
-0.4372
-0.4109
-0.3779
-0.3475
-0.3264
-0.2944
-0.2609
-0.2399
-0.2147
-0.1942
-0.1641
-0.1413
-0.1117
-0.0899
-0.0692
-0.0446
-0.0318
-0.0106
0.0074
0.0129
0.0306
0.0477
0.0576
0.0682
0.0837
0.1118
0.1344
0.1426
0.1405
0.1445
0.1473
0.1288
0.1244
0.1251
0.1306
0.1250
0.1259
0.1268
0.1353
0.1494
0.1455
0.1425

0.1444
0.1519
0.1544
0.1393
0.1353
0.1191
0.1186
0.1120
0.0915
0.0636
0.0489
0.0373
0.0380
0.0330
0.0611
0.0738
0.0792
0.0876
0.0937
0.0996
0.0984
0.1023
0.1044
0.1076
0.1114
0.1046
0.0922
0.0905
0.0949
0.0927
0.0868
0.0691
0.0665
0.0831
0.1128
0.1342
0.1633
0.1758
0.1877
0.1848
0.1919
0.1992
0.1987
0.2018
0.2051
0.2138
0.2154
0.2155
0.2335
0.2589
0.2756
0.2888
0.2980
0.3256

0.3583
0.3932
0.4224
0.4335
0.4343
0.4261
0.4191
0.4152
0.4138
0.4145
0.4137
0.4194
0.4163
0.4236
0.4277
0.4373
0.4407
0.4433
0.4439
0.4281
0.4100
0.4079
0.4210
0.4287
0.4187
0.3802
0.3653
0.3697
0.3905
0.4074
0.4226
0.4387
0.4469
0.4572
0.4747
0.4922
0.4924
0.5051
0.5111
0.5166
0.5175
0.5056
0.5008
0.5021
0.5134
0.5173
0.5141
0.4970
0.4913
0.4914
0.5006
0.4813
0.4657
0.4431

0.4210
0.4069
0.3948
0.3790
0.3718
0.3641
0.3408
0.3267
0.3098
0.2938
0.2758
0.2588
0.2639
0.2672
0.2633
0.2567
0.2483
0.2378
0.2309
0.2187
0.2052
0.2105
0.2152
0.2028
0.1880
0.1817
0.1737
0.1621
0.1593
0.1487
0.1322
0.1304
0.1255
0.1215
0.1179
0.1131
0.1103
0.1029
0.0863
0.0657
0.0420
0.0267
0.0155
0.0065
-0.0104
-0.0252
-0.0443
-0.0551
-0.0678
-0.0775
-0.0907
-0.1047
-0.1207
-0.1377

-0.1518
-0.1661
-0.1843